Open
ORIGINAL ARTICLE

Cell Research (2016) 26:1079-1098.
www.nature.com/cr

Identification of blood vascular endothelial stem cells by the expression of protein C receptor

Qing Cissy Yu[1], Wenqian Song[1], Daisong Wang[1], Yi Arial Zeng[1]

[1]*The State Key Laboratory of Cell Biology, CAS Center for Excellence in Molecular Cell Science, Institute of Biochemistry and Cell Biology, Shanghai Institutes for Biological Sciences, Chinese Academy of Sciences, Shanghai 200031, China*

Vascular growth and remodeling are dependent on the generation of new endothelial cells from stem cells and the involvement of perivascular cells to maintain vessel integrity and function. The existence and cellular identity of vascular endothelial stem cells (VESCs) remain unclear. The perivascular pericytes in adult tissues are thought to arise from the recruitment and differentiation of mesenchymal progenitors during early development. In this study, we identified Protein C receptor-expressing (Procr$^+$) endothelial cells as VESCs in multiple tissues. Procr$^+$ VESCs exhibit robust clonogenicity in culture, high vessel reconstitution efficiency in transplantation, long-term clonal expansion in lineage tracing, and EndMT characteristics. Moreover, Procr$^+$ VESCs are bipotent, giving rise to *de novo* formation of endothelial cells and pericytes. This represents a novel origin of pericytes in adult angiogenesis, reshaping our understanding of blood vessel development and homeostatic process. Our study may also provide a more precise therapeutic target to inhibit pathological angiogenesis and tumor growth.

***Keywords*:** vascular endothelial stem cell; Procr; lineage tracing; bipotent; mammary gland
Cell Research (2016) **26**:1079-1098. doi:10.1038/cr.2016.85; published online 1 July 2016

Introduction

Vascular growth and remodeling are continuous processes vital for development and homeostasis. Angiogenesis, the process that generates new vessels from pre-existing vessels, persists throughout development, coordinated with organ growth and repair. The walls of stable blood vessels are composed of two distinct cell types: endothelial cells (ECs) and pericytes. ECs form a monolayer of vascular tubes, while pericytes associate with and cover the outside of the endothelial tube. The roles of pericytes in angiogenesis are proven to be critical, including physical vessel stabilization [1], blood flow regulation [2, 3] and participation in vascular development and maturation [4-6]. Pericytes are commonly categorized as a subtype of perivascular cells. It is widely recognized that pericytes have mesenchymal or hematopoietic origin and that they are recruited to endothelial tubes [7-11].

ECs are the fundamental building blocks of the vascular architecture. It remains unclear how the EC pool is replenished during homeostasis, i.e., whether it is from the contribution of mature EC proliferation, or the result of vascular stem/progenitor cell activities. The existence and cellular identity of vascular endothelial stem cells (VESCs) also remain controversial. Earlier reports suggest that VESCs originate from circulating bone marrow-derived "endothelial progenitor cells" [13-15]. More recent studies indicate that circulating "endothelial progenitor cells" contribute to vascular endothelium neither in development [16] nor in tumor growth [17]. These studies suggest the existence of resident stem cells in the vascular wall, yet the definitive cellular origin of VESCs for adult angiogenesis has remained unclear. A previous study has implicated c-Kit$^+$ vascular cells as VESCs in the lung using *in vitro* colony formation and *in vivo* transplantation assays [18]. It is known that the above assays may stimulate plasticity as cells are taken away from their native habitats [19], thereby genetic fate mapping (*in vivo* lineage tracing) is needed for the identification of VESCs and interrogation of their properties. It is essential to demonstrate that putative VESCs have

Correspondence: Yi Arial Zeng
Tel: +86-21-5492-1433; Fax: +86-21-5492-1225
E-mail: yzeng@sibcb.ac.cn
Received 29 April 2016; revised 20 May 2016; accepted 25 May 2016; published online 1 July 2016

the ability to give rise to mature endothelial cells both in regeneration and in development, and to establish that putative VESCs encompass two key characteristics that functionally define tissue stem cells: ability to self-renew for a prolonged period, and ability to differentiate into all mature cell types within the tissue [12].

Protein C receptor (Procr), also known as EPCR, is a single-pass transmembrane protein expressed in ECs, with established roles in anticoagulation and inflammation [20-22]. Procr has also been implicated as a marker for murine hematopoietic stem cells [23], and mammary epithelial stem cells [24]. In this study, we sought to investigate the potential of Procr-expressing ECs with regard to their contribution to blood vessel development and regeneration.

Results

Procr-expressing EC populations are enriched for stem cells with regenerative capacity

The growth of an organ requires formation of vasculature, which channels vital oxygen, nutrients and defence cells of the immune system. The mammary gland develops mostly in the postnatal stage, which provides an ideal tissue model to study adult angiogenesis. During puberty, the mammary epithelium undergoes robust extension across the fat pad. We observed that this is a process accompanied by extensive vascularization and vessel remodeling. In a 4-week-old female, the anterior region of the inguinal fat pad is devoid of epithelium (named "empty fat pad") and possesses predominantly capillaries, indicated by the expression of endothelial marker CD31 (PECAM1; Figure 1A). In contrast, at 8 weeks when the epithelium has occupied the fat pad, large blood vessels have also formed in alignment with newly established epithelial branches, with capillaries closely wrapping around the epithelial trunk (Figure 1B). These observations suggest vigorous vascular formation during mammary development, which can be employed to study angiogenesis. We analyzed the location of Procr-expressing cells in the endothelium using immunohistochemical analyses. In the pubertal mammary gland where robust angiogenesis occurs, Procr expression was observed in both tip cells and stalk cells (Figure 1C and 1D); while in the adult mammary gland, Procr$^+$ cells were predominantly found in stalk cells (Figure 1D). The EC identity of Procr$^+$ cells was validated by co-staining with EC markers, including Cdh5 (VE-cadherin), CD31 and Emcn (Endomucin; Figure 1D, Supplementary information, Figure S1A and S1B), and with the EC basement membrane proteins laminin and CoIIV (Supplementary information, Figure S1C and S1D). Next, we analyzed the percentage of Procr-expressing cells in ECs using fluorescence-activated cell sorting (FACS). Single cells were isolated from 8-week-old mouse mammary glands, and ECs were detected using blood lineage$^-$ (CD3e$^-$, Ly6G$^-$/Ly6C$^-$, CD11b$^-$, Gr1$^-$, CD45R$^-$/B220$^-$, Ter119$^-$), CD105$^+$, CD31$^+$ labels [18] (Figure 1E). We found that Procr labels about 4% of ECs (Figure 1E). Sca1$^+$ ECs have been reported to enrich for VESCs [25-27]. We found that the majority of ECs are Sca1$^+$ (85.2% ± 3.3%; Supplementary information, Figure S1E) and Procr$^+$ ECs are included in the Sca1$^+$ population (Supplementary information, Figure S1F). It has been reported that VESCs in the lung can be enriched by using the expression of c-Kit [18]. We found that in the mammary vasculature, c-Kit indeed labels a small population of ECs (2.0% ± 0.3%; Supplementary information, Figure S1E). Notably, c-Kit$^+$ ECs do not overlap with Procr$^+$ ECs (Supplementary information, Figure S1G), suggesting that these are distinct cell populations.

Next, we assessed the regenerative capacity of Procr$^+$ ECs in transplantation assays. Procr$^+$ and Procr$^-$ ECs were isolated from adult *Actin-GFP* mice, mixed with Matrigel and engrafted subcutaneously into recipient nude mice in limiting dilution (illustrated in Figure 1F). At 3 weeks post transplantation, the Matrigel plugs were retrieved and the formation of GFP$^+$ blood vessels was scored. We categorized the extent of vessel growth depending on the overall area of the Matrigel plug being occupied. We observed that Procr$^+$ ECs have drastically higher vessel-forming potential than Procr$^-$ ECs (Figure 1G). Transplanted Procr$^-$ ECs infrequently produced partial vessel outgrowth with limited extension (Figure 1G). In our study, c-Kit$^+$ cells fall into the Procr$^-$ population that has low vessel-forming capacity, raising the question whether c-Kit$^+$ cells are enriched for VESCs in mammary vasculature. To address this, we isolated Procr$^+$ ECs and c-Kit$^+$ ECs from *Actin-GFP* mammary vasculature and performed subcutaneous transplantation in limiting dilution. Consistent with our earlier results, Procr$^+$ ECs readily reconstituted new vessels, whereas c-Kit$^+$ ECs had markedly lower *in vivo* regenerative capacity (Supplementary information, Figure S1H). In colony formation assays described later, Procr$^+$ ECs formed more colonies compared to c-Kit$^+$ ECs, while both populations are more clonogenic than the c-Kit$^-$, Procr$^-$ ECs (Supplementary information, Figure S1I).

We noticed that the majority of vessels formed in our transplantation assays and other reports were small vessels resembling the capillary plexus [18, 28], probably due to the isolated environment in the Matrigel plug. We sought to evaluate the angiogenic capacity of Procr$^+$ ECs by transplanting them back to the developing mammary

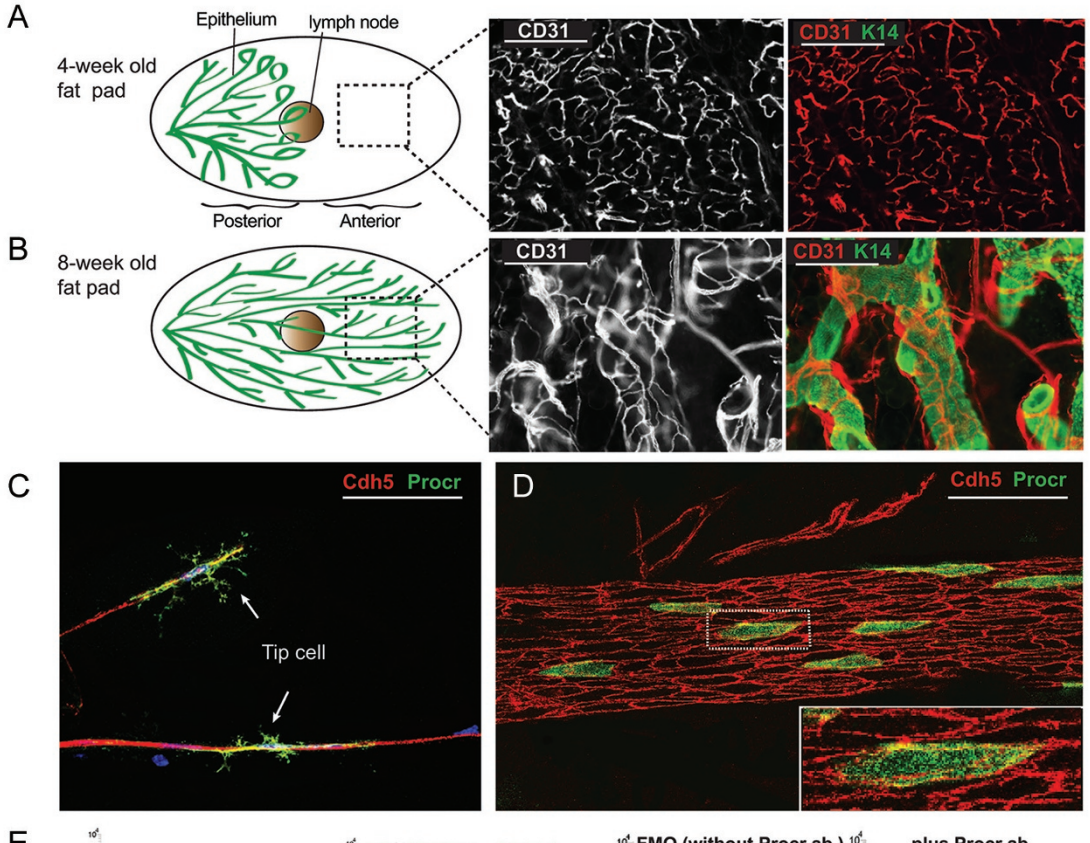

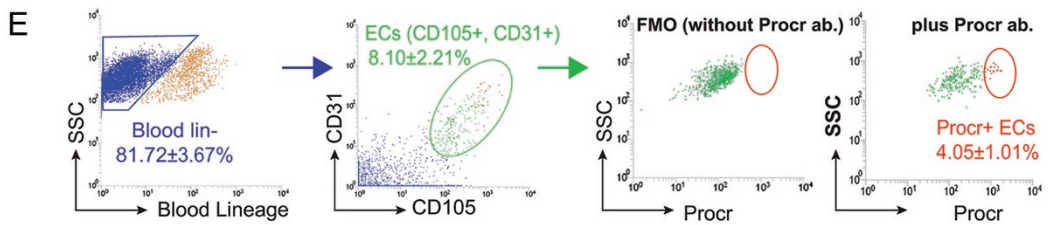

F

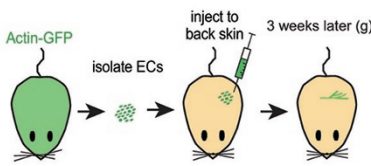

G

Population	Cell no.	Outgrowth	Matrigel plug filled
Lin-, CD105+, CD31+, **Procr+**	15,000	2/2	● 2
	10,000	4/4	● 4
	5,000	4/4	● 4
	3,000	4/4	● 4
	1,000	3/4	● 2 ◔1 ○1
Lin-, CD105+, CD31+, **Procr-**	15,000	1/3	◔ 1 ○2
	10,000	0/3	○ 3
	5,000	0/3	○ 3

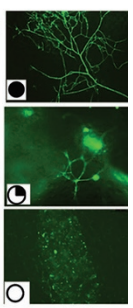

H

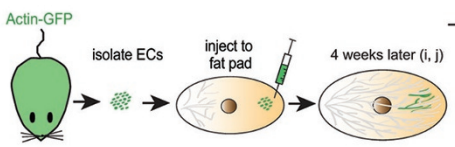

I

Population	Cell no.	Outgrowth
Lin-,CD105+, CD31+, **Procr+**	10,000	4/4
	5,000	2/4
Lin-,CD105+, CD31+, **Procr-**	10,000	0/3
	5,000	0/4

J

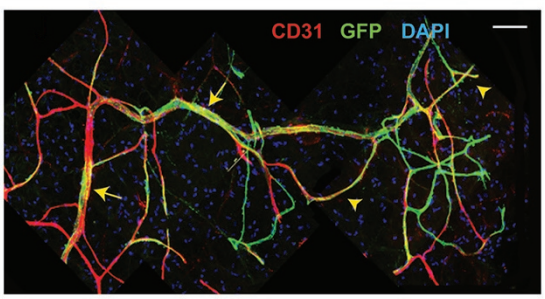

gland. Procr$^+$ ECs were isolated from 8-week-old *Actin-GFP* mouse mammary vasculature, injected into the empty fat pad of pubertal recipients (3-week-old), and harvested 4 weeks later (illustrated in Figure 1H). We expected that the robust mammary development during the period (3-7 weeks) could reveal the angiogenic potential of Procr$^+$ ECs. Indeed, we observed the incorporation of GFP$^+$ ECs into large vessels (Figure 1I and 1J, arrows), and also the formation of secondary and tertiary GFP$^+$ vessel branches (Figure 1J, arrowheads) in an orderly manner. In contrast, Procr$^-$ ECs could neither incorporate into the existing vessels nor form new vessels in mammary fat pads (Figure 1I). Together, our data suggest that Procr$^+$ ECs are enriched for stem cells with robust regenerative capacity.

Procr$^+$ ECs have robust clonogenicity and their stem cell capacity can be retained in culture

We next examined the behavior of Procr$^+$ ECs *in vitro*. We isolated Procr$^+$ and Procr$^-$ ECs, and cultured them in a monolayer as previously established [18]. We found that freshly isolated Procr$^+$ ECs undergo a stable increase in cell number, and can be propagated for at least 10 passages and more than 3 months (Figure 2A). These serially passaged cells largely maintained endothelial properties by showing positive uptake of Acetylated low-density lipoprotein (Ac-LDL), endothelial nitric oxide synthase (eNOS) synthesis, nitric oxide (NO) release and ICAM1 expression upon IL-1β stimulation [29] (Figure 2B and Supplementary information, Figure S2A and S2B). In contrast, Procr$^-$ ECs had a limited ability to be passaged in culture and deteriorated within 3-4 passages (Figure 2A). Notably, cultured Procr$^-$ ECs remained Procr$^-$, while cultured Procr$^+$ ECs gave rise to mostly Procr$^+$ cells and some Procr$^-$ cells as indicated by FACS analyses (Figure 2C).

Next we examined colony-forming ability using 3D culture. Procr$^+$ and Procr$^-$ ECs were FACS-isolated and seeded in 3D methylcellulose culture. We found that Procr$^+$ ECs have drastically higher clonogenicity compared with Procr$^-$ ECs (Figure 2D and 2E), and form a "cordlike" structure as previously described [28, 30] (Supplementary information, Figure S2C and S2D). After 14 days in methylcellulose culture, these colonies interconnected and formed a vascular sheet (Supplementary information, Figure S2E). Colonies formed from Procr$^+$ ECs were dissociated into single cells before being re-plated into fresh methylcellulose. These colonies were capable of generating secondary colonies (Supplementary information, Figure S2F). In contrast, Procr$^-$ ECs rarely formed colonies in culture and these colonies were smaller in size than Procr$^+$ colonies and could not be passaged (Figure 2D and 2E). As mentioned above, Procr$^+$ ECs generated both Procr$^+$ and Procr$^-$ ECs in culture (Figure 2C). These culture-derived Procr$^-$ ECs lost the colony-forming ability, while their Procr$^+$ ECs counterpart retained clonogenicity (Figure 2F).

To address whether the cultured Procr$^+$ ECs retain their stem cell properties, we transplanted the third passage colonies from Procr$^+$ EC culture into empty fat pads and found that, similar to the freshly isolated primary Procr$^+$ ECs, they were able to readily reconstitute blood vessels (8/10, Supplementary information, Figure S2G). To address this at single cell level, we sorted single Procr$^+$ ECs into 96-well plate pre-coated with methylcellulose. Single GFP$^+$ colonies formed from single Procr$^+$ EC were picked and individually transplanted subcutaneously into empty fat pads (illustrated in Figure 2G). GFP$^+$ outgrowths were readily detected in both back skin (9/10) and mammary fat pad (8/10; Figure 2H and 2I). The endothelial identity of these GFP$^+$ vessels was validated by CD31 staining (Figure 2H and 2I). To investigate whether the GFP$^+$ vessels in mammary fat pads are part of functional circulatory vasculature, isolectin was administered by intravenous injection prior to harvest [31]. We observed that the GFP$^+$ vessels were isolectin$^+$,

Figure 1 Procr-expressing endothelial cells are enriched for stem cells with regenerative capacity. **(A)** Illustration of pubertal mammary gland (4-week-old) and staining of endothelium (CD31) and epithelium (outlined by K14) in empty fat pad section prior to epithelial occupancy. Scale bar, 150 μm. **(B)** Illustration of adult mammary gland (8-week-old) and staining of blood vessel (CD31) and epithelium (K14) in section of fat pads with epithelium penetration. Scale bar, 150 μm. **(C**, **D)** Immunohistochemistry indicating the expression of Procr in both tip cells **(C)** and stalk cells **(D)**. Scale bar, 50 μm. **(E)** FACS analysis of Procr expression in 8-week-old C57BL/6 mammary gland ECs. **(F**, **G)** Schematic illustration of subcutaneous transplantation assays. Procr$^+$ ECs and Procr$^-$ ECs were isolated from 8-week-old *Actin-GFP* mammary glands by FACS. The isolated ECs with GFP label were transplanted in limiting dilution into recipients under the flank skin (subcutaneous) as indicated **(F)**. The degree of endothelial vessel outgrowth was evaluated based on the occupancy of Matrigel plug. The representative images were shown on the right. Data were pooled from five independent experiments **(G)**. **(H-J)** Transplantation of sorted Procr$^+$ vs Procr$^-$ ECs in limiting dilution into the empty fat pad of 3-week-old pubertal mammary gland **(H)**. Fat pads of recipients were harvested and the GFP$^+$ vessel outgrowths were analyzed at 4 weeks post transplantation **(I)**. Whole-mount confocal image indicating the integration and contribution of transplanted Procr$^+$ ECs (GFP$^+$) to host mammary vasculature. Endothelial cells were counterstained with CD31 **(J)**. Scale bar, 50 μm.

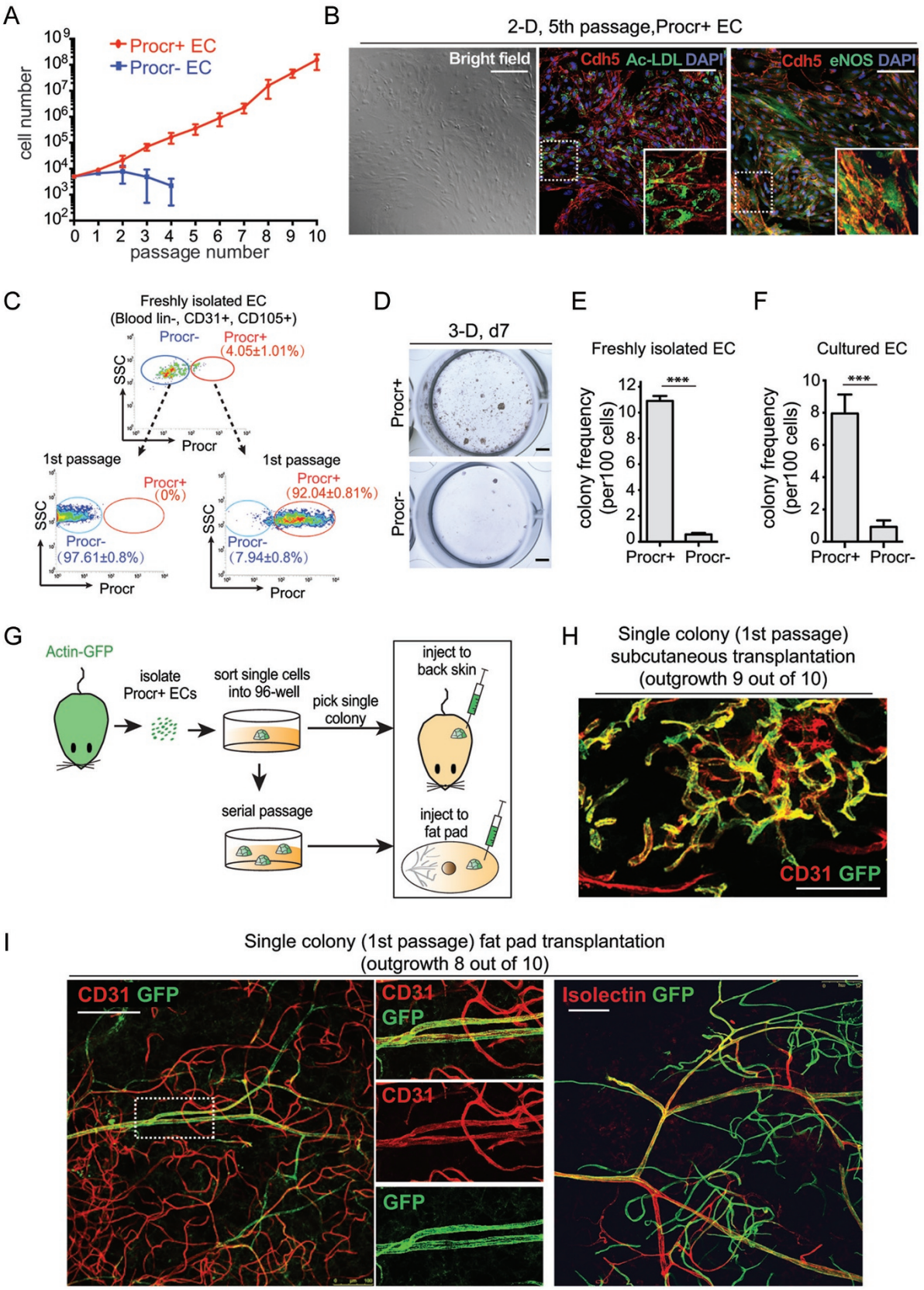
A
Procr+ EC
Procr- EC
cell number
passage number
B
2-D, 5th passage,Procr+ EC
Bright field
Cdh5 Ac-LDL DAPI
Cdh5 eNOS DAPI
C
Freshly isolated EC
(Blood lin-, CD31+, CD105+)
Procr-
Procr+
(4.05±1.01%)
SSC
Procr
1st passage
Procr+
(0%)
Procr-
(97.61±0.8%)
1st passage
Procr+
(92.04±0.81%)
Procr-
(7.94±0.8%)
D
3-D, d7
Procr+
Procr-
E
Freshly isolated EC
colony frequency
(per100 cells)
***
Procr+
Procr-
F
Cultured EC
colony frequency
(per100 cells)
***
Procr+
Procr-
G
Actin-GFP
isolate
Procr+ ECs
sort single cells
into 96-well
pick single
colony
inject to
back skin
serial passage
inject to
fat pad
H
Single colony (1st passage)
subcutaneous transplantation
(outgrowth 9 out of 10)
CD31 GFP
I
Single colony (1st passage) fat pad transplantation
(outgrowth 8 out of 10)
CD31 GFP
CD31
GFP
Isolectin GFP

indicating that they are luminized and connected with the host vasculature (Figure 2I). As mentioned above, Procr$^+$ ECs generated both Procr$^+$ and Procr$^-$ ECs in culture. To further discern the contribution of Procr$^+$ and Procr$^-$ cells upon transplantation, Procr$^+$ and Procr$^-$ cells were isolated from the Procr$^+$ EC culture and transplanted (Supplementary information, Figure S2H). We observed that these culture-derived Procr$^-$ cells lost the regenerative capacity, while their Procr$^+$ counterparts could still readily generate new vessels (Supplementary information, Figure S2H). These results suggest that Procr$^+$ ECs can generate Procr$^+$ descendants that retain stem cell properties following cell culture.

In addition to the mammary vasculature, we also examined the behavior of Procr$^+$ ECs in the skin. A similar percentage of Procr$^+$ ECs (8.8% ± 0.4%) was observed following FACS analysis of abdominal skin endothelium (Supplementary information, Figure S3A). Isolated Procr$^+$ ECs from the skin were able to expand in 2D culture and they maintained their endothelial properties as shown by Ac-LDL uptake, NO release and ICAM1 expression upon stimulation, whereas Procr$^-$ ECs had limited growth in culture (Supplementary information, Figure S3B-S3E). Procr$^+$ ECs from the skin also had significantly higher colony formation ability in 3D culture (Supplementary information, Figure S3F), as well as *in vivo* vessel formation ability compared with Procr$^-$ ECs (Supplementary information, Figure S3G). Together, these results suggest that skin and mammary gland Procr$^+$ ECs are enriched for stem cells with robust colony and blood vessel formation abilities.

Procr$^+$ ECs contribute to EC expansion in lineage tracing

Next we examined the contribution of Procr$^+$ ECs under physiological conditions by *in vivo* genetic fate mapping. We used a *Procr$^{CreERT2\text{-}IRES\text{-}tdTomato/+}$* knock-in mouse model, in which a *CreERT2-IRES-tdTomato* cassette is inserted after the first ATG codon of *Procr* [24]. By crossing the *Procr$^{CreERT2\text{-}IRES\text{-}tdTomato/+}$* allele (*Procr$^{CreERT2/+}$*) with the *Rosa26$^{mTmG/+}$* (*R26$^{mTmG/+}$*) reporter strain [32], we were able to trace the fate of endogenous Procr$^+$ ECs *in vivo* by GFP expression (Figure 3A). We first tracked the developmental fate of Procr$^+$ ECs by administering tamoxifen (TAM) to *Procr$^{CreERT2/+}$;R26$^{mTmG/+}$* pubertal mice (5-week-old) and analyzing the labeled cells both at short term (2 days) and at extended time periods (up to 10 months; Figure 3B). Expression of GFP was not detected in un-induced mice (data not shown). Short-term tracing analyses (2 days) using confocal whole-mount imaging enabled visualization of single GFP-labeled cells on pre-existing blood vessels (Figure 3C and 3D). After 7 and 14 days of tracing, the GFP$^+$ cells expanded in number (Figure 3E-3H). We continued to observe clonal expansion after 2 months of tracing (Figure 3I). Cdh5 and laminin staining validated the endothelial identity of GFP$^+$ cells (Figure 3J and 3K). Quantifying the number of cells in each clone at each analysis time point, ranging from 1 cell at 2 days to about 12 cells at 2 months, further demonstrated the expansion of clone sizes during development (Figure 3L). When the tracing was extended to 10 months, we frequently found that large GFP$^+$ clones constituted entire vessels (Figure 3M and 3N). At this stage it is likely that some neighboring clones have merged, interfering with a precise quantification of cells within individual clones. Together, these data suggest that Procr$^+$ ECs are stem cells that contribute to EC expansion in normal development.

Of note, at the start of TAM induction (5-week), the forefront of the epithelium was at a position slightly past

Figure 2 Procr$^+$ ECs have robust clonogenicity and their cultured progenies retain stem cell capacities. **(A**, **B)** Procr$^+$ ECs and Procr$^-$ ECs were sorted from 8-week-old mammary fat pads and plated in 2-D culture in equal amount. Cell numbers at each passage were quantified and displayed as mean ± SD. Data are pooled from 6 independent experiments **(A)**. Cultured Procr$^+$ ECs (left, bright field) showed positive uptake of Ac-LDL (middle) and positive staining for eNOS Ser1117 **(**right, **B)**. Scale bar, 100 μm. **(C)** Cultured Procr$^+$ ECs or Procr$^-$ ECs from the first passage were subjected to FACS analysis for the expression of Procr. Procr$^-$ ECs remained negative for Procr expression in culture. Procr$^+$ ECs gave rise to majority of Procr$^+$ cells and a small percentage of Procr$^-$ cells as indicated. **(D)** Sorted Procr$^+$ ECs or Procr ECs from 8-week-old CD1 mammary vasculature were cultured in semi-solid 3D methylcellulose medium. Representative pictures of formed colonies on day 7 were shown. Scale bar, 1 mm. **(E**, **F)** Quantification of colony forming frequencies of Procr$^+$ EC or Procr$^-$ EC freshly isolated from the mammary gland **(E)**, and from cultured Procr$^+$ ECs **(F)**. Colony numbers were counted on day 7. Data are pooled from 3 independent experiments and displayed as mean ± SD. ***P < 0.01. **(G)** Schematic illustration of transplantation assays using colonies derived from single Procr$^+$ ECs. **(H)** Single colonies derived from single GFP-labeled Procr$^+$ ECs were mixed with Matrigel and subcutaneously transplanted to recipients. The outgrowths were analyzed at 3 weeks post injection by whole-mount staining with EC marker CD31. GFP$^+$ endothelia were detected in 9 out of 10 Matrigel plugs. Scale bar, 50 μm. **(I)** Single colonies derived from single GFP-labeled Procr$^+$ ECs were transplanted to empty mammary fat pads. The outgrowths were analyzed at 4 weeks post injection by whole-mount staining with EC marker CD31 (left). GFP$^+$ endothelia were detected in 8 out of 10 fat pads. Intravenous injection in recipient mice with isolectin and the following staining indicated that the outgrowths have formed luminized vessels (right). Scale bar, 50 μm.

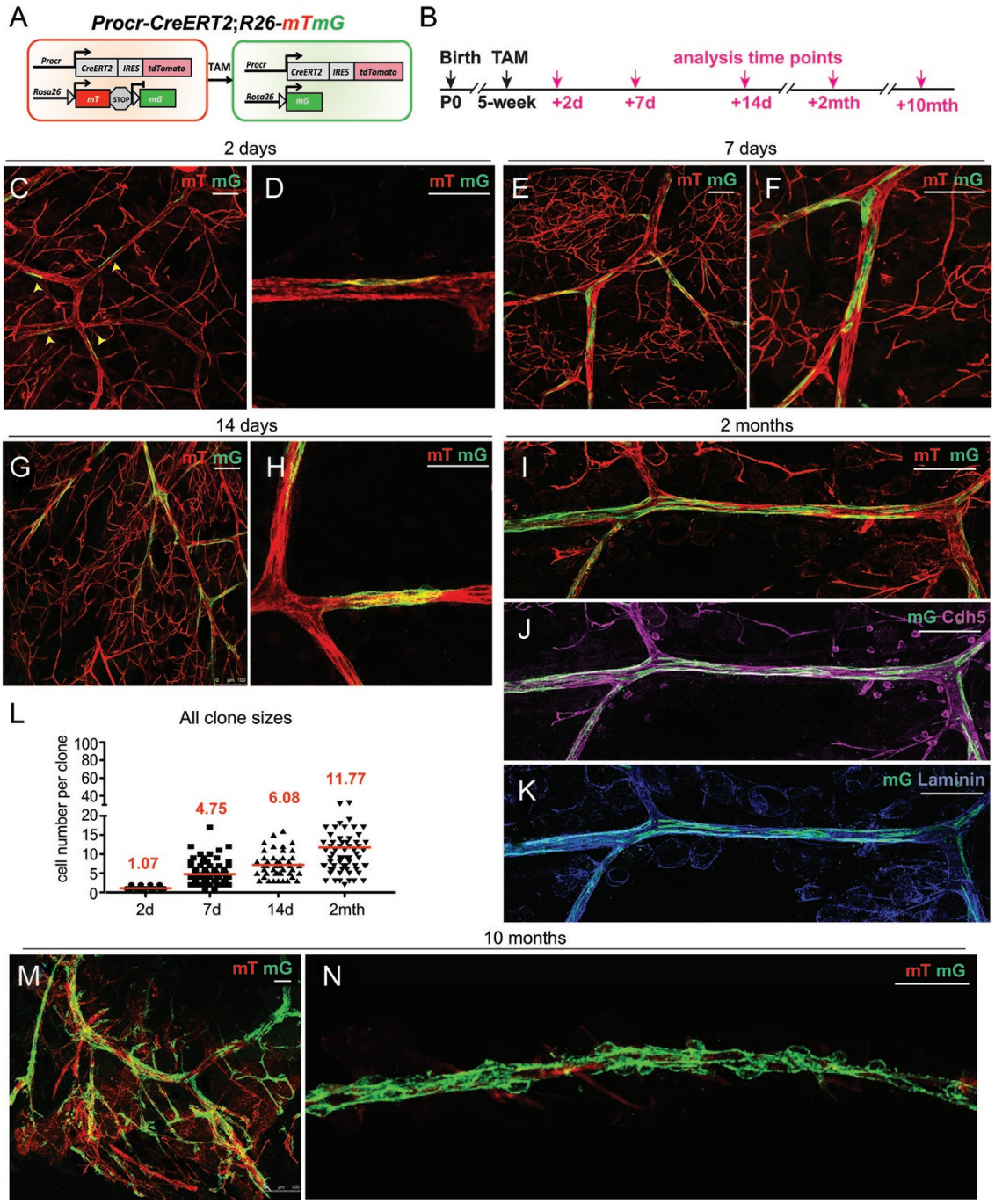

Figure 3 Lineage tracing of Procr^{+} ECs demonstrates their contribution to EC clonal expansion during development. **(A)** Illustration of lineage tracing strategy using *Procr*$^{CreERT2/+}$*;R26*$^{mTmG/+}$ line. **(B)** Experimental setup used in short-term (2 days) and long-term tracing (7 days to 10 months) as indicated. **(C**, **D)** Whole-mount confocal imaging of mammary vasculature at 2 days post TAM administration showing individual GFP^{+} ECs on existing vasculature with zoom out **(C)** and zoom in **(D)** views. Scale bar, 50 μm. **(E-H)** Whole-mount confocal imaging of mammary vasculature at 7 days **(E**, **F)** and 14 days **(G**, **H)** post TAM administration indicating clonal expansion of GFP^{+} cells. Scale bar, 50 μm. **(I-K)** Whole-mount confocal imaging of mammary vasculature at 2 months post TAM administration. Staining of Cdh5 **(J)** and laminin **(K)** confirmed the EC identity of GFP^{+} clones. Scale bar, 50 μm. **(L)** Quantification of cell numbers per GFP^{+} clone indicating the expansion of clone sizes at 2 days, 7 days, 14 days and 2 months post TAM treatment. Data were pooled from at least 3 mice for each tracing time point and are presented as mean ± SD. **(M**, **N)** Whole-mount confocal imaging of mammary vasculature at 10 months post TAM administration.

the lymph node; after 14 days of tracing, the forefront of the epithelium has finished its extension, reaching the other end of the fat pad (illustrated in Figure 1A and 1B, and Supplementary information, Figure S4A). Given the results in Figure 1A and 1B, at this stage the anterior compartment hosts more newly formed vasculature, while the region posterior to the lymph node represents less dynamic, more established vessel development. We quantified the sizes of GPF$^+$ clones in these two compartments, and observed that anterior clones (6.44% ± 0.38% cells per clone) are larger than the posterior clones (3.79% ± 0.27% cells per clone; Supplementary information, Figure S4B), in line with the idea that angiogenesis is more robust in the anterior region.

Next we examined the contribution of Procr$^+$ ECs by carrying out lineage tracing in 8-week-old adult mice (Supplementary information, Figure S4C). Consistently, we observed a significant increase in clone size between tracing done for 2 days and for 2 months (Supplementary information, Figure S4D-S4F). Notably, the GFP$^+$ clone sizes induced from adult tracing were relatively smaller compared with the ones induced in pubertal tracings (8.8 cells per clone in adult tracing at 2 months compared to 11.8 cells per clone in pubertal tracing at 2 months; Supplementary information, Figure S4D and Figure 3L), consistent with the notion of slower vascular turnover in the adult mammary gland.

Lineage tracing reveals that Procr$^+$ ECs can give rise to pericytes

When analyzing GFP$^+$ clones in the previous tracing experiments, to our surprise, we observed the presence of GFP$^+$ pericytes (see below), suggesting that either Procr also labels pericytes, or that Procr$^+$ ECs give rise to new pericytes during the tracing period. Thus we investigated whether Procr$^+$ cells express the pericyte marker nerve/glial antigen-2 (NG2) [33]. FACS analyses demonstrated that neither all ECs (grey, blood lin$^-$, CD31$^+$, CD105$^+$) nor Procr$^+$ ECs (red, blood lin$^-$, CD31$^+$, CD105$^+$, Procr$^+$) express the pericyte marker NG2 (Figure 4A). Co-staining of Procr and NG2 further supported the conclusion; no overlap of Procr$^+$ ECs with NG2$^+$ pericytes was detected (Figure 4B, n > 200 Procr$^+$ ECs scored). Of note, pericytes do not express CD31 and CD105, and should appear in the non-EC fraction that includes stromal cells. Since Procr labels some stromal cells [24], we next examined the Procr$^+$ cells in relation to pericytes in the non-EC compartment (blood lin$^-$, CD31$^-$, CD105$^-$). FACS analyses indicated that Procr$^+$ cells and pericytes (NG2$^+$, Pdgfrb$^+$) [34] are two distinct populations with no overlap in this compartment (Figure 4C), suggesting that pericytes do not express Procr.

We next investigated whether Procr$^+$ ECs give rise to new pericytes using lineage tracing. First, we used *Procr$^{CreERT2/+}$;R26$^{mTmG/+}$* mice and initiated the tracing by TAM administration at 5 weeks. We examined the Procr$^+$ cell distribution in mammary vasculature over time. At 2 days post TAM induction, consistent with previous results (Figure 3C and 3D), the majority of GFP-labeled ECs remained as single-cell clones (94.5% out of > 200 GFP$^+$ clones scored, n = 6 mammary glands from 3 independent experiments). All GFP$^+$ cells are CD31$^+$ ECs and do not express the pericyte marker NG2 (Figure 4D). In *Procr$^{CreERT2/+}$;R26$^{mTmG/+}$* mammary glands examined 2 months after induction of tracing, we observed the presence of GFP$^+$ pericytes within GFP$^+$ clones using the pericyte marker NG2 (arrowheads in Figure 4E and Supplementary information, Figure S5A). The appearance of GFP$^+$ pericytes was further confirmed by using additional pericyte markers, Desmin [35] (Figure 4F), αSMA [36] (Supplementary information, Figure S5B) and Pdgfrb (Supplementary information, Figure S5C). Moreover, laminin staining indicated that the GFP$^+$ pericytes and the GFP$^+$ ECs share the same basement membrane, further validating the pericyte identity of the GFP$^+$, αSMA$^+$ cells (Supplementary information, Figure S5D). Quantification of GPF$^+$ pericytes seen in GFP$^+$ clones in each analysis time point indicated that the frequency of pericyte(s) labeling increased over time, from 0% at 2 days to 16.1% at 2 months to 32.1% at 10 months (Figure 4G). Notably, we were only able to detect GFP$^+$ pericytes on smaller vessels. We speculated that it could be because large vessels have functionally matured prior to the initiation of tracing, thereby no pericyte differentiation occurs during the tracing period. FACS analyses further supported the appearance of GFP$^+$ pericytes and their increasing number over time. We first quantified the percentage of GFP$^+$ ECs, which allowed us to determine the overall labeling efficiency and expansion of clones in these experiments. The percentage of GFP$^+$ ECs started from 0.86%, and increased to 8.51% at 2 months and 23.49% at 10 months (Figure 4H and Supplementary information, Figure S6A). This is consistent with the increasing clone sizes described above (Figure 3L). Quantification of pericytes by FACS demonstrated increasing numbers of GFP$^+$ pericytes during the tracing time, from 0% at 2 days to 2.98% at 2 months to 7.06% at 10 months (Figure 4I and Supplementary information, Figure S6B). Together, these results suggest that more pericytes had been generated from Procr$^+$ ECs over time.

To further validate the Procr$^+$ EC origin of pericytes, we used the multicolor *R26R-Confetti* (*R26^{Confetti}*) reporter [37]. TAM injection in *Procr$^{CreERT2/+}$;R26$^{Confetti/+}$* mice allows Procr$^+$ cells to randomly adopt one of the four flu-

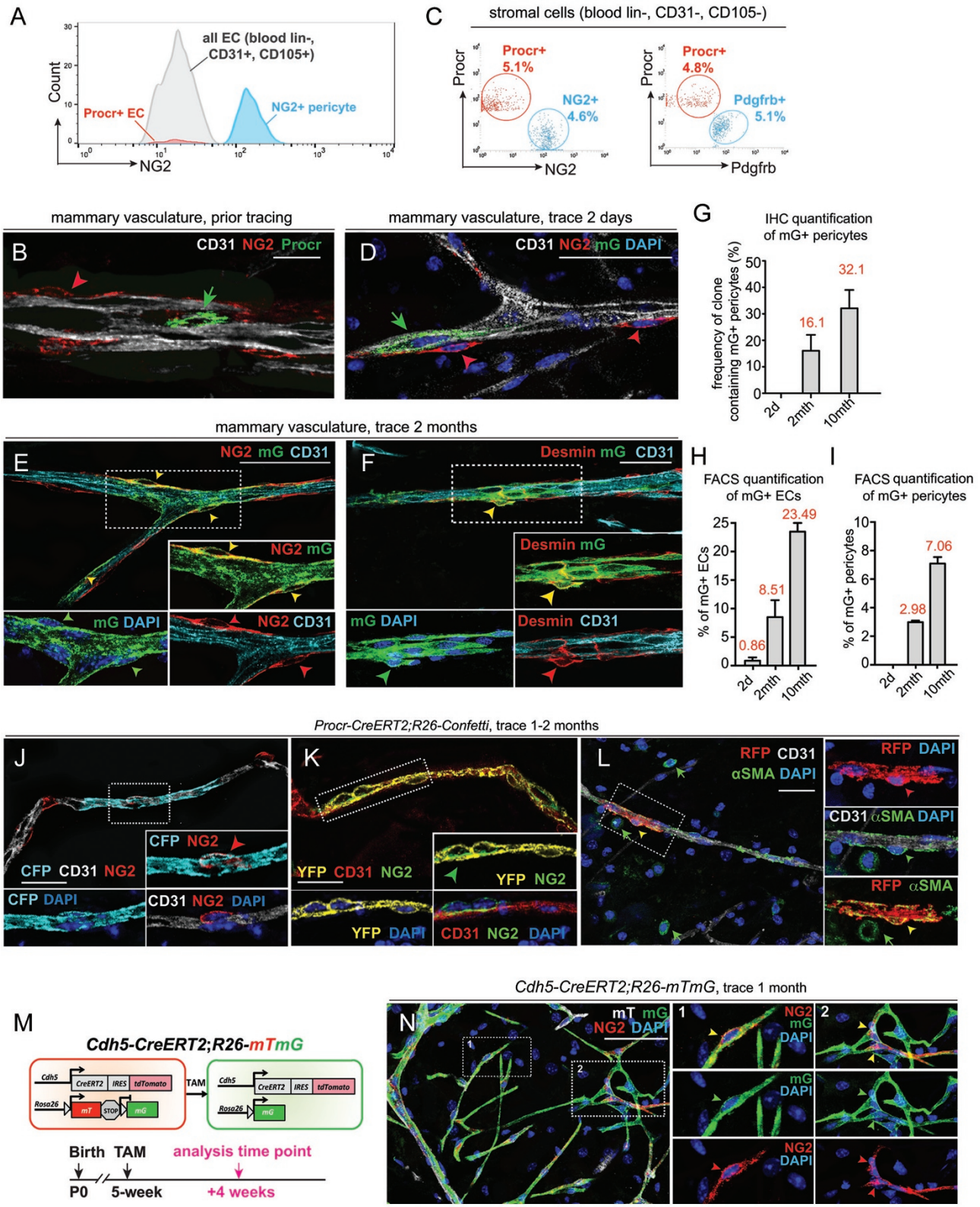
A
all EC (blood lin-, CD31+, CD105+)
Procr+ EC
NG2+ pericyte
Count
NG2
C
stromal cells (blood lin-, CD31-, CD105-)
Procr+ 5.1%
NG2+ 4.6%
Procr+ 4.8%
Pdgfrb+ 5.1%
Procr
NG2
Pdgfrb
mammary vasculature, prior tracing
B
CD31 NG2 Procr
mammary vasculature, trace 2 days
D
CD31 NG2 mG DAPI
G
IHC quantification of mG+ pericytes
frequency of clone containing mG+ pericytes (%)
32.1
16.1
2d
2mth
10mth
mammary vasculature, trace 2 months
E
NG2 mG CD31
NG2 mG
mG DAPI
NG2 CD31
F
Desmin mG CD31
Desmin mG
mG DAPI
Desmin CD31
H
FACS quantification of mG+ ECs
% of mG+ ECs
23.49
8.51
0.86
I
FACS quantification of mG+ pericytes
% of mG+ pericytes
7.06
2.98
Procr-CreERT2;R26-Confetti, trace 1-2 months
J
CFP NG2
CFP CD31 NG2
CFP DAPI
CD31 NG2 DAPI
K
YFP CD31 NG2
YFP NG2
YFP DAPI
CD31 NG2 DAPI
L
RFP CD31 αSMA DAPI
RFP DAPI
CD31 αSMA DAPI
RFP αSMA
M
Cdh5-CreERT2;R26-mTmG
Cdh5
CreERT2
IRES
tdTomato
Rosa26
mT
STOP
mG
TAM
Birth
TAM
analysis time point
P0
5-week
+4 weeks
Cdh5-CreERT2;R26-mTmG, trace 1 month
N
mT mG
NG2 DAPI
1
NG2 mG DAPI
mG DAPI
NG2 DAPI
2

orescent colors. We initiated the tracing at 5 weeks and analyzed the contribution of Procr$^+$ ECs after 4-8 weeks. We detected the presence of pericytes within single *Confetti* color clones (CFP, YFP or RFP; arrowheads in Figure 4J-4L), and pericyte(s) always exhibited the same labeling color as the ECs, indicating that they share the same cellular origin. To be noted, no surrounding fibroblasts were labeled with the same color (Figure 4L), minimizing the possibility that these labeled pericytes were recruited from surrounding fibroblasts or generated by other Procr$^+$ stem cells. These data further demonstrate the *de novo* formation of pericytes from local Procr$^+$ ECs.

Next we investigated the formation of pericytes using another Cre line, Cdh5-CreER [38]. Cdh5 is broadly expressed in ECs and its expression is restricted in ECs. We administered TAM to *Cdh5-CreERT2;R26*$^{mTmG/+}$ pubertal mice (5-week-old) and analyzed the labeled cells on mammary vasculature after 4 weeks of tracing (illustrated in Figure 4M). We observed the presence of GFP$^+$ pericytes, indicating the EC origin of these pericytes (Figure 4N). Thus, with two independent Cre lines, our data demonstrate the *de novo* formation of pericytes from local ECs.

We analyzed vessel outgrowths in the previously described transplantation assays (Figures 1J and 2I), in which Procr$^+$ ECs isolated from *Actin-GFP* mice were injected, and also observed the presence of GFP$^+$ pericytes marked by NG2 expression (Supplementary information, Figure S5E). These data indicate that the GFP$^+$ pericytes are donor-derived from transplanted Procr$^+$ ECs (GFP$^+$), not through recruitment from recipient tissues (GFP$^-$). In addition, we analyzed the formation of pericytes in cultured ECs. Both immunostaining and FACS analyses supported the idea that Procr$^+$ ECs can generate pericytes *in vitro* (Supplementary information, Figure S5F and S5G), whereas Procr$^-$ ECs cannot (Supplementary information, Figure S5H).

Procr expression marks bipotent VESCs in multiple tissues

Our *in vitro* culture, transplantation and lineage tracing experiments all suggest that Procr$^+$ ECs are stem sells in mammary vasculature. Next we investigated the contribution of Procr$^+$ ECs in the vasculature of other adult tissues, including the skin and retina. Labeling was initiated in 5-week-old *Procr*$^{CreERT2/+}$*;R26*$^{mTmG/+}$ mice, and abdominal skin and retinas were harvested at 2 days and 2 months post TAM induction (Figure 5A). In short-term (2 days) tracing, labeled cells were predominantly single ECs in the skin vasculature (Figure 5B), and we found no overlap of GFP$^+$ ECs with pericytes (Supplementary information, Figure S7B). After 2 months of tracing, clones with increased cell numbers were detected (Figure 5C and 5D). FACS analyses of the skin vasculature revealed that the percentage of GFP$^+$ ECs started from 3.4% at 2 days, and increased to 9.91% at 2 months and to 29.79% at 10 months (Figure 5E and Supplementary information, Figure S6C). Pericyte formation was also observed in the skin vasculature. At 2 months of tracing, GFP$^+$ pericytes were readily detected in Procr$^+$ EC-derived clones (Figure 5F and Supplementary information, Figure S7C). The frequency of pericyte(s) seen in GFP clones increased from 0% at 2 days to 21.73% at 2 months (Figure 5G). Quantification of pericytes by FACS also demonstrated the overall percentage of labeled pericyte increased from 0% at 2 days, to 2.04% at 2 months and 9.09% to 10 months (Figure 5H and Supplementary information, Figure S6D).

Figure 4 Procr$^+$ VESCs contribute to pericyte formation. **(A)** FACS analysis indicating that neither all ECs (grey) nor Procr$^+$ ECs (red) express pericyte marker NG2. Pericyte was used as a positive control for NG2 expression (blue). **(B)** Whole-mount immunohistochemistry of mammary vasculature confirming that Procr$^+$ ECs (Procr$^+$, CD31$^+$, arrow) do not overlap with pericytes (NG2$^+$, arrowhead). *n* = 206 Procr$^+$ cells scored. Scale bar, 50 μm. **(C)** FACS analysis of the stromal cell compartment indicating that pericytes (blue, marked by NG2$^+$ or Pdgfrb$^+$) and Procr-expressing fibroblasts (red) are distinct populations. **(D)** Whole-mount analysis of mammary vasculature at 2 days post TAM induction showing a GFP$^+$ EC (arrow) and GFP$^-$ pericytes (arrowheads). Scale bar, 50 μm. **(E**, **F)** Whole-mount analysis of mammary vasculature at 2 months post TAM induction showing that a GFP$^+$ clone consisted of both ECs (CD31$^+$) and pericytes marked by NG2 (arrowheads in **E**) or Desmin (arrowheads in **F**). Scale bar, 50 μm. **(G)** Quantification of the percentage of clones containing GFP$^+$ pericytes. 16.1% of clones contained GFP$^+$ pericyte at 2 months of tracing, and the percentage increased to 32.1% at 10 months of tracing. Data are presented as mean ± SD. Data were pooled from at least 3 mice for each tracing time point. **(H**, **I)** Quantification of GFP$^+$ ECs and GFP$^+$ pericytes in the mammary gland by FACS analysis, indicating the growing percentage of GFP$^+$ ECs **(H)** and GFP$^+$ pericytes **(I)** as tracing period prolongs. **(J**-**L)** Whole-mount confocal images indicating that CFP **(J)**, YFP **(K)** or RFP **(L)** labeled clone consisted of both ECs (CD31$^+$) and pericytes (αSMA$^+$ or NG2$^+$) after 1-2 months of tracing. CFP, cyan fluorescent protein; RFP, red fluorescent protein; YFP, yellow fluorescent protein. Scale bar, 50 μm. **(M)** Illustration of lineage tracing strategy using *Cdh5-CreERT2;R26*$^{mTmG/+}$ line and experimental setup used. **(N)** Whole-mount confocal image of *Cdh5-CreERT2;R26*$^{mTmG/+}$ mammary vasculature at 4 weeks post TAM administration. Boxed area showed GFP$^+$ pericytes (arrowheads, NG2$^+$ cells) within GFP$^+$ endothelial clones. Scale bar, 50 mm.

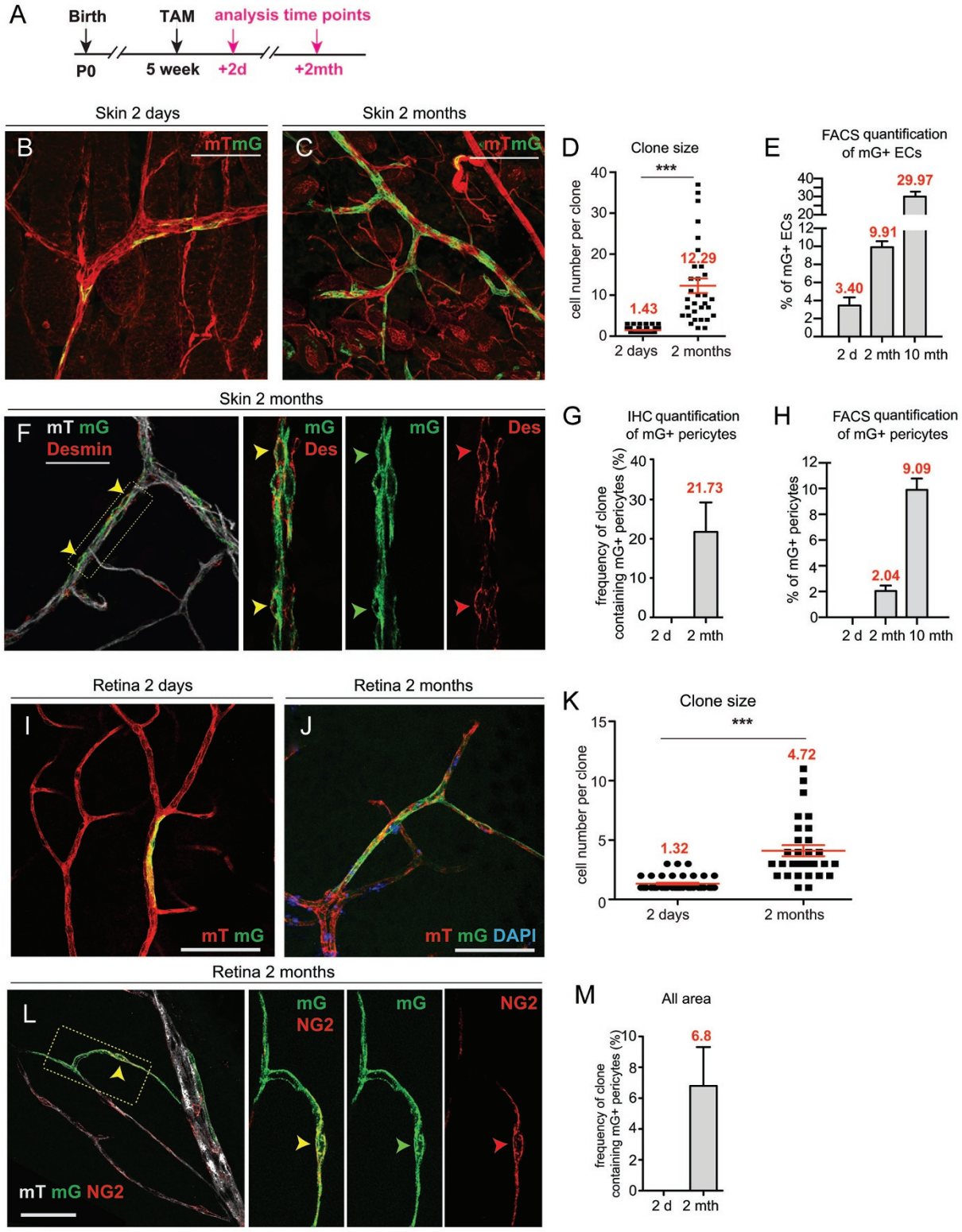
A
Birth
TAM
analysis time points
P0
5 week
+2d
+2mth
Skin 2 days
Skin 2 months
B
mTmG
C
mTmG
D
Clone size
***
cell number per clone
1.43
12.29
2 days
2 months
E
FACS quantification of mG+ ECs
% of mG+ ECs
3.40
9.91
29.97
2 d
2 mth
10 mth
Skin 2 months
F
mT mG
Desmin
mG
Des
mG
Des
G
IHC quantification of mG+ pericytes
frequency of clone containing mG+ pericytes (%)
21.73
2 d
2 mth
H
FACS quantification of mG+ pericytes
% of mG+ pericytes
2.04
9.09
2 d
2 mth
10 mth
Retina 2 days
Retina 2 months
I
mT mG
J
mT mG DAPI
K
Clone size
***
cell number per clone
1.32
4.72
2 days
2 months
Retina 2 months
L
mT mG NG2
mG
NG2
mG
NG2
M
All area
frequency of clone containing mG+ pericytes (%)
6.8
2 d
2 mth

In retinal vasculature short-term tracing experiments, labeled cells were also predominantly single ECs in the retina (Figure 5I), and no overlap of GFP$^+$ ECs with pericytes was observed (Supplementary information, Figure S7D). After 2 months of tracing, clone sizes expanded (Figure 5J and 5K), and GFP$^+$ pericytes appeared (Figure 5L and Supplementary information, Figure S7E and S7F). Laminin staining confirmed that the GFP$^+$ pericytes and the GFP$^+$ ECs share the same basement membrane (Supplementary information, Figure S7G). The frequency of pericyte(s) seen in GFP clones increased from 0% at 2 days to 6.8% at 2 months (Figure 5M). Notably, the clones in the retina (Figure 5K) were smaller in size compared to the ones in the skin (Figure 5D), consistent with the notion of a slower turnover rate of the retina compared with the skin. Together, these results suggest that Procr$^+$ ECs act as stem cells that can generate both ECs and pericytes, and this could be a shared cellular mechanism in vasculatures of many organs.

Procr$^+$ VESCs are crucial for blood vessel development and regeneration

To evaluate the functional importance of Procr$^+$ VESCs during vascular development, we performed targeted ablation of these cells in the developing retina. Retinal vasculature develops postnatally in a tightly regulated temporal and spatial pattern that can readily be observed. The superficial vascular vessels develop immediately after birth by radial outgrowth of the vessels from the centre of the optic disc to the periphery, reaching the retinal edges at approximately postnatal day 8, covering the superficial layer of the retina by forming a 2-D vascular structure [39]. We generated a *Procr$^{CreERT2/+}$;R26$^{DTA/+}$* strain to conditionally express diphtheria toxin (DTA) in Procr$^+$ cells. This allowed us to determine the requirement for Procr$^+$ cells in retinal development. TAM was administered on day 1.5 and the retinas were harvested on day 6 (Figure 6A). We found that, compared to the control (*R26$^{DTA/+}$*), vascular development was severely delayed in *Procr$^{CreERT2/+}$;R26$^{DTA/+}$* retinas, with vessel extension reaching only ~50% of the entire retina diameter (Figure 6B and 6C). Of note, the phenotype of delayed development is likely because the efficiency of TAM-mediated recombination and cell ablation did not reach 100%. As a result, the remaining Procr$^+$ VESCs escaped from the ablation and contributed to the partial development. These experiments suggest that Procr$^+$ VESCs are important for normal retinal vascular development.

Next we investigated the regenerative potential of Procr$^+$ VESCs in vascular injury repair using a limb ischemia model. Hind limb ischemic injuries were induced in recipient mice by occlusion of the femoral artery, and mice were allowed to recover for 2 days after surgery. At that point, Procr$^+$ ECs or Procr$^-$ ECs were isolated from donor *Actin-RFP* mice and transplanted intramuscularly into the ischemic limbs. Laser Doppler analyses of blood flow were performed on day 2 and day 23 post surgery (Figure 6D). On day 23, mice treated with Procr$^+$ ECs demonstrated significantly improved blood flow compared with the control animals that were treated with Procr ECs (Figure 6F-6H). Immunohistochemistry of the limb treated with Procr$^+$ ECs revealed the formation of RFP$^+$ blood vessels, validating the contribution of the donor cells (Figure 6I). Isolectin staining indicated that those RFP$^+$ vessels are connected to the main circulation (Figure 6J). These results suggest that Procr$^+$ VESCs are effective in vascular restoration upon injury.

Procr$^+$ VESCs display angiogenic and EndMT molecular signatures

To investigate the properties of Procr$^+$ VESCs, we performed RNA sequencing (RNA-seq) analysis on iso-

Figure 5 Procr$^+$ VESCs contribute to both EC and pericyte formation in the skin and retina vasculature. **(A)** Experimental setup used in skin and retina vasculature lineage tracing. **(B**, **C)** Whole-mount confocal imaging of the abdominal skin vasculature showing individual GFP$^+$ cells at 2 days after TAM administration **(B)**, and GFP$^+$ clones at 2 months after TAM induction **(C)**. Scale bar, 100 μm. **(D)** Quantification of cell numbers per GFP$^+$ clone at each time point indicating the expansion of clone sizes. **(E)** FACS analysis indicating the increasing percentage of GFP$^+$ ECs. **(F)** At 2 months post TAM induction, the clones contained pericytes marked by Desmin (Des; arrowheads). Scale bar, 100 μm. **(G)** Quantification of the percentage of GFP$^+$ clones that contained GFP$^+$ pericytes. No clones contained GFP$^+$ pericyte at 2 days of tracing, and the percentage increased to 21.73% at 2 months of tracing. **(H)** FACS quantification confirmed the increasing percentage of GFP$^+$ pericytes as tracing period prolongs. Data were pooled from at least 3 mice for each tracing time point and are presented as mean ± SD. **(I**, **J)** Whole-mount confocal imaging of the retina vasculature showing individual GFP$^+$ cells at 2 days after TAM administration **(I)**, and GFP$^+$ clones at 2 months after TAM induction **(J)**. Scale bar, 50 μm. **(K)** Quantification of cell numbers per GFP$^+$ clone at each time point indicating the expansion of clone sizes. **(L)** At 2 months post TAM administration, the GFP$^+$ clones contained pericytes marked by NG2 **(**arrowhead**)**. Scale bar, 50 μm. **(M)** Quantification of the percentage of GFP$^+$ clones that contained GFP$^+$ pericytes. When analyzed in all area, no clones contained GFP$^+$ pericyte at 2 days of tracing, and the percentage increased to 6.8% at 2 months of tracing. Data were pooled from at least 3 mice for each tracing time point and are presented as mean ± SD.

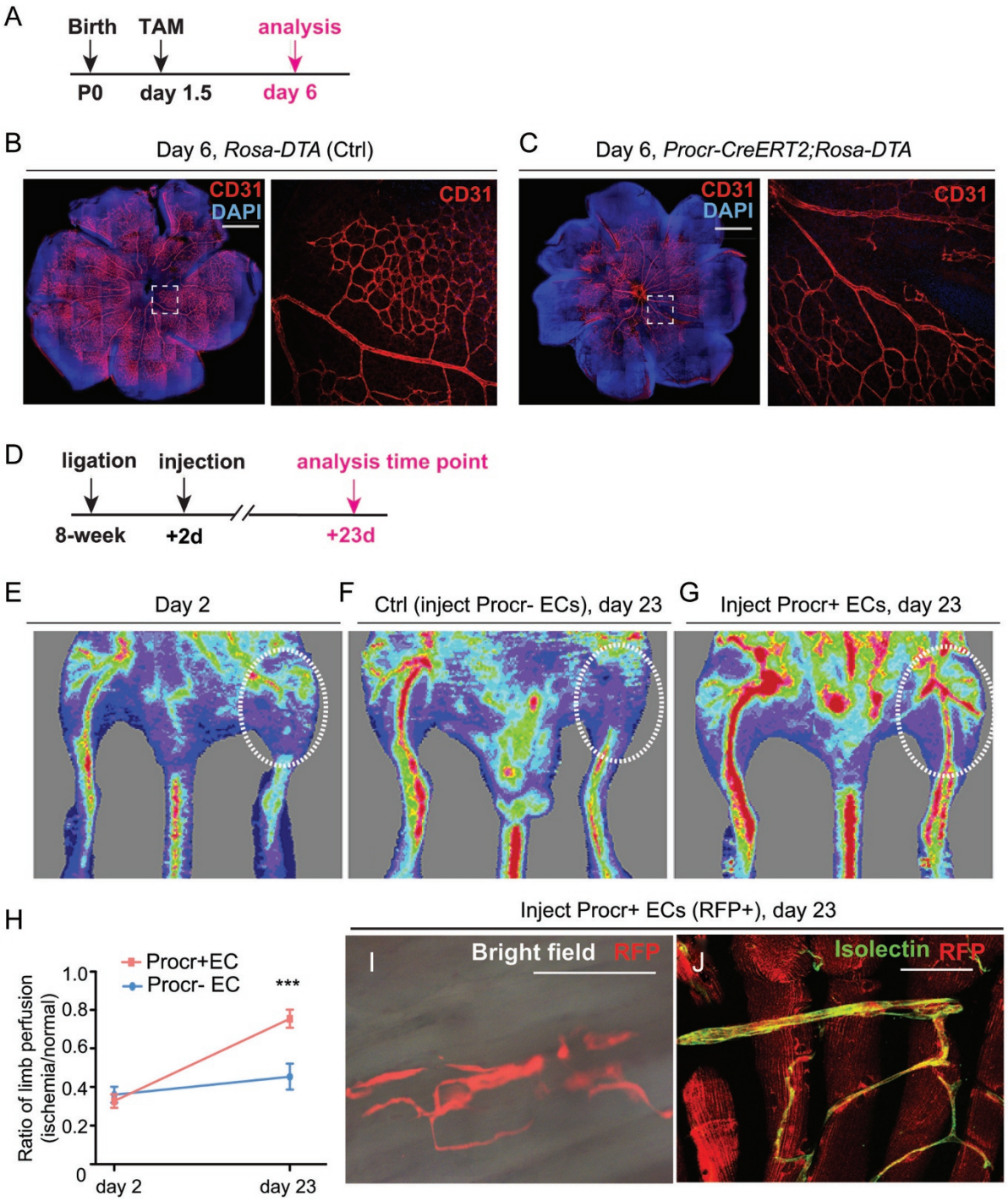

Figure 6 Procr^{+} VESCs are crucial for vascular development and regeneration. **(A-C)** Targeted ablation of Procr^{+} cells delays retina blood vessel development. *Procr*$^{CreERT2/+}$*;R26*$^{DTA/+}$ mice and *R26*$^{DTA/+}$ mice (Ctrl) were TAM administered at postnatal day 1.5 and retinas were harvested on day 6 as illustrated **(A)**. The whole-mount view of entire retinal vascular occupancy as well as zoom-in view of vascular structure were visualized by CD31 whole-mount staining **(B, C)**. Scale bar, 500 μm. **(D-J)** Mice were subjected to femoral artery ligation followed by intramuscular injection with Procr^{+} ECs or Procr^{-} ECs isolated from *Actin-RFP* mice on day 2. Representative laser-Doppler perfusion imaging of mice on day 2 **(E)** and day 23 **(F, G)** after hind limb ischemia is shown. Quantification of blood flow recovery was calculated from > 3 mice/group (n = 3 in Procr^{-} EC group, n = 5 in Procr^{+} EC group). Data are presented as mean ± SD. ***P < 0.01 **(H)**. Whole-mount microscopy image visualizing the formation of RFP^{+} vessel in mice receiving Procr^{+} EC injection on day 23 **(I)**. Confocal image confirming that these RFP^{+} vessels are connected to the systemic circulation as evidenced by isolectin staining **(J)**. Scale bar, 50 μm.

lated Procr$^+$ and Procr$^-$ ECs from mammary vasculature. We found that Procr$^+$ VESCs have higher expression of genes that have been implicated in angiogenesis and vascular development (Figure 7A), including surface receptors such as *Vegfr1*, *Vegfr2*, *Tie1*, *Tie2*, *Notch1*, and *Notch3*, potentially sensitizing VESCs' responsiveness to angiogenic stimuli. Many angiogenesis-related secreted molecules, transcription factors and adhesion molecules were also upregulated in Procr$^+$ VESCs. These observations were validated by qPCR experiments (Figure 7B-7E). Interestingly, Procr$^+$ VESCs exhibit characteristics of endothelial-to-mesenchymal transition (EndMT; Figure 7F). This is consistent with the postulation that a partial EndMT is required for initiating angiogenic sprouting [40]. In addition to the previously reported EndMT signatures [41], characteristic genes of epithelial-to-mesenchymal transition (EMT), e.g., *Zeb1*, *Zeb2*, *Foxc2* and *Vimentin* were upregulated in Procr$^+$ VESCs (Figure 7F and 7G). Consistently, transcription factors that are suppressed in EMT, e.g., *Ovol1* and *Ovol2* were downregulated in Procr$^+$ VESCs (Figure 7G). To further validate these results, we performed immunostaining analysis of Zeb1, a central mediator of EMT [42]. We observed that Procr$^+$ VESCs indeed express Zeb1 (Figure 7H). Zeb1 is also expressed in perivascular cells as expected (Figure 7H). EndMT has been regarded as a subtype of EMT [43]. Analyses in Procr$^+$ VESCs suggest that EndMT and EMT share more similarities in molecular signature than previously known.

Discussion

Identifying bipotent VESCs

Although much effort has been devoted to identifying the cellular origin of ECs [18, 25-28], the existence and the identity of VESCs remain elusive, due to the lack of *in vivo* evidence. Our study identifies Procr as a novel marker for VESCs through *in vitro* analyses and *in vivo* lineage tracing. Procr$^+$ VESCs have robust clonogenicity in culture and vigorous vessel formation capability in transplantation. Procr$^+$ VESCs actively contribute to the development and maintenance of homeostasis in postnatal angiogenesis in mammary, skin and retina vasculatures. In line with the robustness of tissue turnover, Procr$^+$ VESCs are more active in skin vasculature compared to the others, generating more descendent cells as evidenced by bigger clones in each assessed tracing period. In multiple adult tissues, Procr$^+$ VESCs are bipotent, giving rise to new ECs and pericytes during development. This model argues against the current paradigm of a linear endothelial lineage, adding a subset of pericytes under the endothelial stem cell hierarchy. Transcriptome analysis indicates the prominent EndMT and EMT features of these VESCs. This is reminiscent of the EMT characteristic identified in Procr$^+$ mammary epithelial stem cells [24], and may indicate a shared feature of these Procr-labeled adult stem cells.

Pathological vs physiological EndMT

EndMT is the process by which endothelial cells lose their cell-specific markers and morphology, and acquire a mesenchymal cell-like phenotype. EndMT has been observed in a range of pathological conditions. In cardiac fibrosis model, a lineage tracing study using *Tie1-Cre* mice (*Tie1* gene encodes a pan-endothelial cell marker) has demonstrated the significant contribution of vessel ECs to cardiac fibrotic tissue and scar formation through EndMT [44]. In vein grafting, a common revascularization surgery for patients suffering from coronary disease, the formation of aberrant aortic smooth muscle cell-like neointima through EndMT is associated with grafting failure [45]. EndMT has also been observed in the brain ECs in the context of cerebra cavernous malformation (CCM), a vascular dysplasia [41]. In heterotopic ossification disorders, ECs undergoing EndMT could acquire a mesenchymal stem cell-like phenotype, capable of differentiating into osteoblasts, chondrocytes and adipocytes [46]. *In vitro*, EndMT has also been documented in aortic ECs under the influence of Wnt7b signaling [47]. The above observations exemplify the potential of endothelial (stem) cells in pathological conditions and their plasticity in the *in vitro* setting. The true cell fate of endothelial (stem) cells, however, may only be manifested *in vivo* at certain windows during normal development. Our lineage tracing studies provide direct evidence that Procr$^+$ VESCs give rise to pericytes in normal development and homeostasis.

The current study not only identifies a novel source of pericytes, but also brings new insight into the cellular mechanism during pathological processes. For example, in fibrotic kidney disease, lineage tracing studies propose that pericytes were progenitors of myofibroblasts, which contribute to renal fibrosis [48, 49]. In light of our lineage tracing studies, it is possible that VESCs are the cells of origin of organ fibrosis under pathological conditions. The EndMT signatures that Procr$^+$ VESCs carry could be advantageous for the mesenchymal fate switching during normal development (to become pericytes) or during pathological process (to further become fibroblasts).

Diverse cellular origin of pericytes

Pericytes displayed heterogeneity in their phenotype, distribution and origin [50-52]. The reported diverse

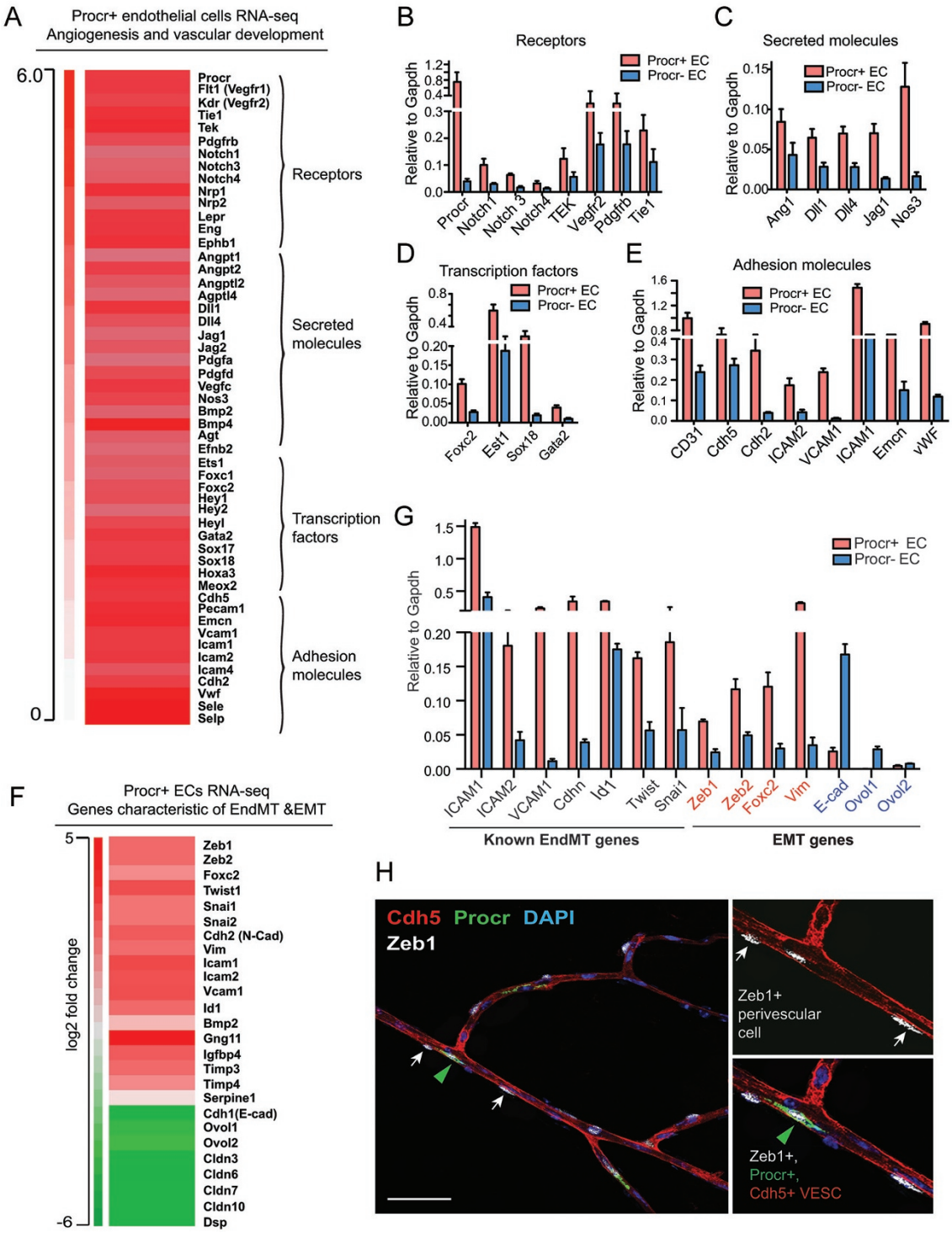

Figure 7 Procr^{+} VESCs have higher expression of angiogenic genes and display EndMT molecular signature. **(A)** RNA-seq analysis indicating upregulation of angiogenesis- and vascular development-related genes in Procr^{+} ECs compared to Procr^{-} ECs. **(B-E)** qPCR validation of RNA-seq results, including cell surface receptors **(B)**, secreted molecules **(C)**, transcription factors **(D)**, and adhesion molecules **(E)** that are involved in angiogenesis and vascular development. **(F)** RNA-seq analysis indicating upregulation of characteristic genes of EndMT and EMT in Procr^{+} VESCs. **(G)** qPCR validation of RNA-seq results showing higher expression of typical EndMT- and EMT-related genes in Procr^{+} VESCs compared to Procr^{-} ECs. **(H)** Whole-mount confocal analysis of mammary vasculature showing Zeb1 staining on perivascular cells (arrows, Cdh5^{-}) and Zeb1 staining on Procr^{+} VESC (Cdh5^{+}, Procr^{-}) as well (green arrowhead). Scale bar, 50 μm.

cellular origin of pericytes is likely reflective of their heterogeneous nature. Early experiments using quail-chick chimera suggest that mural cells and smooth muscle cells in face and forebrain blood vessels are derived from neural crest [53]. Pericytes in the cephalic region are of neuroectodermal origin as demonstrated by lineage tracing using *Sox10-iCreERT2* mice [54]. In the developing liver and lung, mesodermal lineages contribute to pericyte population as indicated by lineage tracing using *Mesp1-Cre* [7], a transiently expressed mesodermal marker in gastrulation, as well as using *Wt1-Cre* [9], which specifically marks mesothelial cells during embryonic stage [55]. Unlike conditional CreER of which the labeling efficiency is dependent on TAM induction efficacy, both of the mesodermal lineage studies have utilized Cre alleles which theoretically are capable of labeling all mesodermal cells, yet in both studies the labeled pericytes are only a portion of total pericytes in the organ, implying that there are other origins for pericytes.

Because of the reported distinct origins of pericytes with ECs, the model that pericytes are recruited to endothelial tubes, which is easy to comprehend, has been widely accepted. The experimental evidence of pericyte recruitment and their subsequent assembly with endothelial tubes is predominantly based on co-culture and co-transplantation assays. Co-culture of embryonic multipotent 10T/12 cells with ECs has led to the differentiation and morphological change of those 10T/12 cells, exhibiting αSMA expression and vessel attachment [8]. More recently, pericyte recruitment is documented in tumor engraftment model. By grafting human osteosarcoma and fibrosarcoma cells into *Desmin-lacZ* mice, host-derived pericytes are observed in the growing tumors [11]. This has been presented as the major evidence of pericyte recruitment. However, ECs in those xenografts are likely also host derived, thereby an alternative explanation can also be that pericytes are derived from recruited ECs.

Accompanied with the recruitment model, it has been proposed that the arriving pericytes interact with local ECs to promote new basement membrane assembly. This is supported by the evidence that increased basement membrane deposition was observed in the co-culture of pericytes and ECs [25, 40]. These interpretations reasonably depict the assembly of newly formed vessels at the tip. However, at established vessels during homeostasis, how the recruited pericytes or their progenitors penetrate through the basement membrane remains to be elucidated. Other mechanisms may exist for EC and pericyte assembly.

Our work provides direct evidence for the *de novo* formation of pericytes from local endothelial stem cells during vessel growth and renewal. These observations may reshape the understanding of blood vessel maturation and repair process.

Mammary fat pat as a new tissue model to study angiogenesis

Unlike other mammalian organs, the mammary gland develops mostly in the postnatal stage. At the onset of puberty, the mammary epithelium proliferates and extends to occupy the whole mammary fat pad. Convoying the establishing epithelium architecture is the robust remodeling of surrounding vascular structures. Thereby, the mammary gland offers an excellent model for the study of angiogenesis, in addition to other conventional tissue models, e.g., skin, retina and lung. Moreover, mammary fat pad is an ideal grafting site for assessing angiogenic potential of exogenous cells. It provides space, matrix and rich angiogenic stimuli from the growing mammary epithelium therein. It also allows the formed exogenous vessels to connect with the host circulation system, enabling a further functional evaluation and representing an advantage over subcutaneous transplantation. Last but not least, mammary fat pad that is outside the peritoneal cavity is very accessible; operation on it introduces limited distresses to the host.

Conclusion

Our study identifies Procr^{+} endothelial cells as bipotent VESCs in multiple vascular systems, and adds an additional local source to the diverse pericyte origin. Our study may provide more precise therapeutic targets to inhibit pathological angiogenesis and tumor growth, as well as provide new insight into the cellular contribution to fibrotic disorders.

Materials and Methods

Experimental animals

Rosa26$^{mTmG/+}$, *Rosa26*$^{DTA/+}$ and Cdh5-CreER (Jackson Laboratories), *Procr*$^{CreERT2\text{-}IRES\text{-}tdTomato}$ [24], *Rosa26R-Confetti* [56], *Actin*$^{GFP/+}$, *Actin*$^{RFP/+}$, CD1, C57BL/6J, and nude strains were used in this study. For lineage tracing experiments induced in pubertal and mature adult mice, animals received a single intraperitoneal injection of 4 mg per 25 g body weight of TAM (Sigma-Aldrich) diluted in sunflower oil. A minimum of three mice were used for each tracing period. To obtain *Procr*$^{CreERT2/+}$*;R26R-Confetti* mice, *R26R-Confetti* mice were crossed with *Procr*$^{CreERT2\text{-}IRES\text{-}tdTomato}$ mice. Random double heterozygous female mice between 5 and 8 weeks old received a three-course (on every second day for a period of 5 days) intraperitoneal injection of 4 mg per 25 g body weight of TAM diluted in sunflower oil to induce activation of Cre recombinase, which in turn induced expression of one of the Confetti colors (nuclear GFP, membranous CFP, cytoplasmic YFP and RFP). To obtain

Procr$^{CreERT2/+}$;*Rosa26*$^{DTA/+}$ mice, *Rosa26*$^{DTA/+}$ mice were crossed with *Procr*$^{CreERT2\text{-}IRES\text{-}tdTomato}$ mice. Random double heterozygous pups received a double dose of intraperitoneal injection of 0.2 mg TAM at postnatal day 1.5 to induce Cre recombinase-mediated cell ablation. Experimental procedures were approved by the Animal Care and Use Committee of Shanghai Institute of Biochemistry and Cell Biology, Chinese Academy of Sciences.

Primary cell preparation and flow cytometry

Primary cell preparation was conducted using previously reported protocol [24]. In brief, mammary glands of 8-week-old female virgin mice were harvested and single-cell suspension was obtained by Collagenase III (Worthington)-mediated digestion of minced tissue, followed by trypsin-EDTA and DNaseI (Sigma) sequential incubation before filtering through 70 μm cell strainers. The following antibodies in 1:200 dilutions were used: rat anti-mouse CD16/CD32 (Mouse BD Fc Block™, BD PharMingen, clone # 2.4G2), FITC-conjugated hematopoietic lineage cocktail (Biolegend, Cat# 133302, cocktail includes antibody against CD3e, Ly-6G/Ly-6C, Gr-1, CD11b, CD45R/B220, and Ter119), APC-conjugated CD31 (BD PharMingen, clone # MEC 13.3), APC-conjugated CD140b (Biolegend, clone # APB5), PE-Cy7-conjugated CD31 (eBiosciences, clone # 390), APC- and PE-conjugated CD105 (eBioscience, clone # MJ7/18), PE-Cy7-conjugated Sca1 (eBioscience, clone # D7), FITC-conjugated c-Kit (BD Biosciences, clone # 2B8) and Procr (eBioscience, clone # eBio1560), APC-conjugated NG2 (Bioss, Cat# bs-4800R-A647), Streptavidin-v450 (BD PharMingen). Antibody incubation was performed on ice for 20 min in PBS with 5% fetal bovine serum (FBS; HyClone, Thermo Scientific). All analysis and sorting were performed using a FACSJazz (Becton Dickinson). The purity of sorted population was routinely checked and ensured to be > 95%. Automated cell deposition unit in FACSJazz was used for single cell sorting of populations onto 96-multiwell plates, and the presence of the sorted cells was ensured using fluorescence microscopy.

Cell culture and in vitro colony formation assay

Freshly isolated endothelial cells were cultured on fibronectin (Sigma)-coated 24-well plates in IMDM medium containing 15% FBS, 1% BSA, 10^{-4} mM 2-mercaptoethanol (Sigma), 1% Glutamax, 1% ITS-X (Insulin, transferrin and Selectin, Life Technologies), 100 ng/ml rmVEGFa (R&D systems) and 50 ng/ml rmbFGF (Life Technologies) at 37 °C in a humidified 5% CO_2 atmosphere (Esco Medical). Cells were passaged using 0.05% trypsin when reaching 80%-90% confluence, fresh medium was supplied every 2-3 days depending on cell confluence. For *in vitro* endothelial cell colony assays, freshly isolated cells were plated in triplicate in 0.5 ml of semi-solid methylcellulose (Stem Cell Technologies), supplemented with 100 ng/ml rmVEGFa. Colonies were scored after 7 days. Passage of primary colonies was achieved by single colony picking using a sterile pipette tip followed by digestion into single-cell suspension using 0.05% trypsin. Single cells were then re-plated into freshly supplemented methylcellulose medium. Colonies containing 10 or more cells were counted. To visualize the overall density of colonies in an entire well, the culture contents were fixed with 4% PFA followed by wash and 30-min incubation with Crystal Violet dye and visualized using Leica MZ FLIII dissection microscope.

Immunohistochemistry

Mammary gland and abdominal skin whole-mount staining was performed as described previously [57] with adjustment to prolong tissue digestion period to better accommodate vasculature visualization. Retina dissection and whole-mount staining preparation was accomplished as previously demonstrated [58]. For immunohistochemistry on cell culture, cells were seeded onto fibronectin-coated 8-well chamber slides (Transwell, Lab-Tek) and allowed to reach confluence. Before antibody staining, cells in the chamber slides were washed with PBS and fixed in cold 4% PFA for 15 min, followed by 20-min permeablization in 0.1% Triton X-100 and 1-h blocking using 10% of appropriate serum in PBS. Frozen sections were prepared by air-drying and fixation for 45 min in cold 4% PFA, followed by the same permeablization and blocking procedures as cell culture. Tissue sections were incubated with primary antibodies at 4 °C overnight, followed by washes, incubation with secondary antibodies for 2 h at room temperature, and counterstained with DAPI (Life Technologies). Representative images were shown in the figures. The primary antibodies used in immunofluorescence were rat anti-mouse CD31 (BD Bioscience, clone # MEC 13.3), rat anti-mouse Cdh5 (BD Biosciences, clone # 11D4.1), rabbit anti-mouse NG2 (Millipore, Cat# AB5320), rabbit anti-mouse Desmin (Millipore, Cat# 04-585), rabbit anti-mouse Collagen Type IV (Millipore, Cat# AB756P), mouse anti-mouse αSMA (Sigma-Aldrich, Cat# A2547), rabbit anti-mouse laminin (Sigma-Aldrich, Cat# L9393), rat anti-mouse Procr (eBioscience, clone # eBio1560), hamster anti-mouse ICAM1 (BD Bioscience, clone # 3E2), rat anti-mouse Endomucin (Santa Cruz, Cat# sc-53941), rabbit anti-mouse Keratin 14 (Covance), rabbit anti-mouse Pdgfrb (Cell Signaling Technology, Cat# 3169), rabbit anti-mouse Phospho-eNOS Ser1177 (Cell Signaling Technology, Cat# 9570), rabbit anti-mouse Zeb1 (Novus Biological, Cat# NBP1-05987), and chicken anti-mouse GFP (Life Technologies, Cat# A10262). The secondary antibodies used were donkey anti-rat Cy3, goat anti-rat Alexa Fluor 488, goat anti-rat Alexa Fluor 647, goat anti-mouse Alexa Fluor 647, goat anti-rabbit Alexa Fluor 647, donkey anti-goat Alexa Fluor 647 (Life Technologies). Fluorescence microscope images were captured using Zeiss AX10 and confocal images were captured using Leica DM6000 TCS/SP8 laser confocal scanning microscope. All presented images were scanned as multiple layers at 1.0 μm thickness each layer and z-stack processed (or 3D construction processed as per specified using Imaris 8.2.0 surface mode) to ensure correct co-localization of fluorescence signals.

Ac-LDL uptake

For analysis of Ac-LDL uptake of endothelial cells in culture, cells were incubated with 10 μg/ml Alexa Fluor 488-labeled Ac-LDL (Life Technologies) for 2 h at 37 °C with 5% CO_2 atmosphere, followed by fixation and immunostaining procedures.

NO detection assays

Passaged blood lin$^-$, CD31$^+$, CD105$^+$, Procr$^+$ EC cultures were used at 70%-80% of confluency. Cells were washed with PBS once and incubated with low-serum (2% FBS) fresh medium supplemented with 10 μM NO indicator DAF-FM Diacetate (Molecular Probes, Life Technologies) and processed according to the manufacturer's instructions. DAF-FM Diacetate excitation/emission maxima is 495/505 nm. Activation of eNOS was detected

by immunofluorescence staining for the activation of Ser1117 site (rabbit anti Phospho-eNOS Ser1117, Cell Signaling), followed by secondary antibody staining using goat anti-rabbit Alexa Fluor 647 (Life Technologies). Fluorescence detection was visualized using Leica TCS/SP8 laser confocal microscope.

Adhesion molecule expression

Adhesion molecule expression was determined in a cell-based ELISA as previously described [29]. In brief, blood lin$^-$, CD31$^+$, CD105$^+$, Procr$^+$ ECs were FACS isolated and plated as monolayer culture in 24-multiwell plates till 70%-80% of confluency. Cultured cells either remained unstimulated or were stimulated with IL-1β (0.1-1 nM) for 24 h at 37 °C. Afterwards cells were washed with PBS and fixed with 2% PFA (pH 7.2). Cells were then processed for immunofluorescence staining with rat anti-mouse ICAM1 (eBioscience) followed by donkey anti-rat Cy3 (Life Technologies). Fluorescence detection was achieved using Leica TCS/SP8 laser confocal microscope.

Quantification of lineage-specific cells and the size of clones

A minimum of three different mice were analyzed per tracing period. Dissociated single mammary cells were FACS analyzed for the composition of endothelial lineage and pericytes. For clonal analysis, a minimum of three experimental mice and a minimum of 100 GFP$^+$ clones were analyzed per time point by whole-mount preparation. For each clone, the number of cells was scored in reference to CD31 or Cdh5 expression to assure their endothelial identity. For scoring of GFP$^+$ pericytes, cells were scored in reference to Pdgfrb, NG2, Desmine and αSMA expression or in relative location to laminin or Collagen IV basement membrane staining. GFP$^+$ pericytes were quantified by two approaches: first as "total clones", that is all counted GFP$^+$ clones regardless of the location and vessel types; second as "pericyte existing area", that is to include GFP$^+$ clones having pericyte located within (GFP$^+$) and clones that have pericyte located nearby (1-3 cell distance to the clone edge, tdTomato$^+$). For clone identification in *Procr*$^{CreERT2/+}$*;R-26R*$^{Confetti/+}$ mice, whole-mount tissue preparation was carried out and cells were scored in reference to the abovementioned endothelial or pericyte markers to assure their cellular identity. Fluorescence microscope images were captured using Leica DM6000 TCS/SP8 laser confocal scanning microscope. All presented images were scanned as multiple layers at 1.0 μm thickness each layer and z-stack processed to ensure correct co-localization of fluorescence signals.

EdU labeling

In vivo EdU labeling was conducted by intraperitoneal injection of EdU mixture at 0.2 mg per 10 g body weight into mice, followed by tissue harvest 2 h after incubation. Samples were subjected to Click-it chemistry (Invitrogen) prior to immunohistochemistry preparation.

In vivo neovascularization using Matrigel

8-week-old C57BL/6J mice were used as recipients. Freshly isolated cell populations were resuspended in 0.4 ml Matrigel (Becton Dickinson) supplemented with 60 units/ml heparin (Sigma) and 150 ng/ml VEGF, and injected subcutaneously into the flank region. Matrigel plug was retrieved and analyzed 3-4 weeks later. Outgrowth were detected under fluorescent microscope (Zeiss) and categorized according to the total filled area of the Matrigel plug.

Mammary fat pad transplantation and analysis

Freshly isolated endothelial populations were resuspended in Matrigel mixture consisting of 50% Matrigel, PBS with 20% FBS, and 0.01% Trypan Blue (Sigma). Total volume of 15 μl was injected into the fat pads of 3-week-old female nude mice. Mammary glands were harvested 4 weeks post transplantation. Donor-derived endothelial outgrowth and host vessel integration were detected after whole-mount preparation and images were captured by confocal microscope (Leica DM6000 TCS/SP8).

Hind limb ischemia model and EC transplantation

8-10-week-old nude mice were anaesthetised with intraperitoneal injection of Avertin. The proximal portions of the right femoral artery as well as the distal portion of the saphenous artery were double occluded and the obstructed portion of the artery was resected. Hind limb muscles were harvested 23 days after induction of ischemia. Controls were subjected to ischemia induction without EC transplantation. For EC transplantation, blood lin$^-$, CD31$^+$, CD105$^+$ Procr$^+$ or Procr$^-$ ECs were sorted from *Actin*$^{RFP/+}$ mice. The hind limb ischemia model was prepared and mice were allowed to rest for 48 h before local ischemic site muscular injection of EC populations.

Laser Doppler blood flow analysis

Hind limb blood flow was measured using a laser Doppler blood flow meter (LDBF; MoorLDI, Moor Instrument). LDBF analyses over the legs and paws were performed on postoperative day 2 and day 23. After scanning, sorted images were analyzed to quantify blood flow, and mean blood flow values of the ischemic and non-ischemic limb were calculated. To maintain consistency of data collection and prevent data variation due to ambient light and termperature, blood flow was expressed as the ratio of the left (non-ischemic) and right (ischemic) hind limb LDBF.

RNA-seq and quantitative real-time PCR analysis

Total RNAs from freshly isolated blood lin$^-$, CD105$^+$, CD31$^+$, Procr$^+$ and blood lin$^-$, CD105$^+$, CD31$^+$, Procr$^-$ ECs were extracted with RNAiso Plus (Takara) following the manufacturer's protocol. Total mRNA concentration was determined with NanoDrop ND-1000 and RNA-seq libraries were prepared according to the manufacturer's instruction (Illumina) followed by sequencing on Illumina HiSeq 2000, which was performed by BG-tech (Beijing Genomics Institute). In total, more than 35 million of 1 × 100 single reads for each sample were obtained and uniquely mapped to the mm9 mouse genome with > 75% mapping rate for both samples. Differential gene expression analysis was carried out and genes with significant alteration were extracted and further analyzed using DAVID Bioinformatics Resources 6.7. RNA-seq data can be viewed online under GEO accession number GSE69129. Expression of selected genes was validated and quantitative RT-PCR was performed using TaqMan gene expression systems for mouse (Applied Biosystems).

Statistical analysis

Student's *t*-test was performed and the *P*-value was calculated in GraphPad PRISM 5.0 on data represented by histograms and dot plots, which consisted of results from at least three indepen-

dent experiments unless specified otherwise. For all experiments with error bars, the standard deviation (SD) was calculated to indicate the variation within each experiment. When only two groups were compared, a two-sided Student's *t*-test was used. *P* value of < 0.05 was considered significant.

Acknowledgments

We are grateful to Drs Esther Verheyen and Chi-Chung Hui for critical reading of the manuscript and all lab members for helpful discussion. We thank Dr Bin Zhou for kindly providing the Cdh5-CreER mouse. We thank Weimin Jiang, Liu Wei, Xiaorui Zhang and Shengkai Zuo for technical assistance. This work was supported by the National Natural Science Foundation of China (31530045 and 31371500 to YAZ, 31401245 to QCY), the Ministry of Science and Technology of China (2014CB964800 and 2012CB945000 to YAZ), the Chinese Academy of Sciences (XDA01010307 to YAZ) and Chinese Society of Cell Biology (Early Career Fellowship to QCY).

Author Contributions

YAZ conceived the study. QCY, WS and DW performed the experiments. YAZ and QCY analyzed the data and wrote the manuscript.

Competing Financial Interests

The authors declare no competing financial interests.

References

1 Diaz-Flores L, Gutierrez R, Varela H, Rancel N, Valladares F. Microvascular pericytes: a review of their morphological and functional characteristics. *Histol Histopathol* 1991; **6**:269-286.
2 Hall CN, Reynell C, Gesslein B, *et al.* Capillary pericytes regulate cerebral blood flow in health and disease. *Nature* 2014; **508**:55-60.
3 Pallone TL, Silldorff EP. Pericyte regulation of renal medullary blood flow. *Exp Nephrol* 2001; **9**:165-170.
4 Hellström M, Gerhardt H, Kalén M, *et al.* Lack of pericytes leads to endothelial hyperplasia and abnormal vascular morphogenesis. *J Cell Biol* 2001; **153**:543-553.
5 Lindahl P, Johansson BR, Leveen P, Betsholtz C. Pericyte loss and microaneurysm formation in PDGF-B-deficient mice. *Science* 1997; **277**:242-245.
6 Simonavicius N, Ashenden M, van Weverwijk A, *et al.* Pericytes promote selective vessel regression to regulate vascular patterning. *Blood* 2012; **120**:1516-1527.
7 Asahina K, Zhou B, Pu WT, Tsukamoto H. Septum transversum-derived mesothelium gives rise to hepatic stellate cells and perivascular mesenchymal cells in developing mouse liver. *Hepatology* 2011; **53**:983-995.
8 Hirschi KK, Rohovsky SA, D'Amore PA. PDGF, TGF-beta, and heterotypic cell-cell interactions mediate endothelial cell-induced recruitment of 10T1/2 cells and their differentiation to a smooth muscle fate. *J Cell Biol* 1998; **141**:805-814.
9 Que J, Wilm B, Hasegawa H, Wang F, Bader D, Hogan BL. Mesothelium contributes to vascular smooth muscle and mesenchyme during lung development. *Proc Natl Acad Sci USA* 2008; **105**:16626-16630.
10 Yamashita J, Itoh H, Hirashima M, *et al.* Flk1-positive cells derived from embryonic stem cells serve as vascular progenitors. *Nature* 2000; **408**:92-96.
11 Abramsson A, Berlin O, Papayan H, Paulin D, Shani M, Betsholtz C. Analysis of mural cell recruitment to tumor vessels. *Circulation* 2002; **105**:112-117.
12 Wagers AJ, Weissman IL. Plasticity of adult stem cells. *Cell* 2004; **116**:639-648.
13 Asahara T, Murohara T, Sullivan A, *et al.* Isolation of putative progenitor endothelial cells for angiogenesis. *Science* 1997; **275**:964-967.
14 Bompais H, Chagraoui J, Canron X, *et al.* Human endothelial cells derived from circulating progenitors display specific functional properties compared with mature vessel wall endothelial cells. *Blood* 2004; **103**:2577-2584.
15 Yoder MC, Mead LE, Prater D, *et al.* Redefining endothelial progenitor cells via clonal analysis and hematopoietic stem/progenitor cell principals. *Blood* 2007; **109**:1801-1809.
16 Rinkevich Y, Lindau P, Ueno H, Longaker MT, Weissman IL. Germ-layer and lineage-restricted stem/progenitors regenerate the mouse digit tip. *Nature* 2011; **476**:409-413.
17 Wojakowski W, Tendera M, Michałowska A, *et al.* Mobilization of CD34/CXCR4+, CD34/CD117+, c-met+ stem cells, and mononuclear cells expressing early cardiac, muscle, and endothelial markers into peripheral blood in patients with acute myocardial infarction. *Circulation* 2004; **110**:3213-3220.
18 Fang S, Wei J, Pentinmikko N, Leinonen H, Salven P. Generation of functional blood vessels from a single c-kit+ adult vascular endothelial stem cell. *PLoS Biol* 2012; **10**:e1001407.
19 Snippert HJ, Clevers H. Tracking adult stem cells. *EMBO Rep* 2011; **12**:113-122.
20 Bae JS, Yang L, Manithody C, Rezaie AR. The ligand occupancy of endothelial protein C receptor switches the protease-activated receptor 1-dependent signaling specificity of thrombin from a permeability-enhancing to a barrier-protective response in endothelial cells. *Blood* 2007; **110**:3909-3916.
21 Fukudome K, Esmon CT. Identification, cloning, and regulation of a novel endothelial cell protein C/activated protein C receptor. *J Biol Chem* 1994; **269**: 26486-26491.
22 Vetrano S, Ploplis VA, Sala E, *et al.* Unexpected role of anticoagulant protein C in controlling epithelial barrier integrity and intestinal inflammation. *Proc Natl Acad Sci USA* 2011; **108**:19830-19835.
23 Balazs AB, Fabian AJ, Esmon CT, Mulligan RC. Endothelial protein C receptor (CD201) explicitly identifies hematopoietic stem cells in murine bone marrow. *Blood* 2006; **107**:2317-2321.
24 Wang D, Cai C, Dong X, *et al.* Identification of multipotent mammary stem cells by protein C receptor expression. *Nature* 2015; **517**:81-84.
25 Hu Y, Zhang Z, Torsney E, *et al.* Abundant progenitor cells in the adventitia contribute to atherosclerosis of vein grafts in ApoE-deficient mice. *J Clin Invest* 2004; **113**:1258-1265.
26 Passman JN, Dong XR, Wu SP, *et al.* A sonic hedgehog signaling domain in the arterial adventitia supports resident Sca1+ smooth muscle progenitor cells. *Proc Natl Acad Sci*

USA 2008; **105**:9349-9354.
27 Sainz J, Al Haj Zen A, Caligiuri G, *et al.* Isolation of "side population" progenitor cells from healthy arteries of adult mice. *Arterioscler Thromb Vasc Biol* 2006; **26**:281-286.
28 Naito H, Kidoya H, Sakimoto S, Wakabayashi T, Takakura N. Identification and characterization of a resident vascular stem/progenitor cell population in preexisting blood vessels. *EMBO J* 2012; **31**:842-855.
29 Patsch C, Challet-Meylan L, Thoma EC, *et al.* Generation of vascular endothelial and smooth muscle cells from human pluripotent stem cells. *Nat Cell Biol* 2015; **17**:994-1003.
30 Zhang XQ, Takakura N, Oike Y, *et al.* Stromal cells expressing ephrin-B2 promote the growth and sprouting of ephrin-B2(+) endothelial cells. *Blood* 2001; **98**:1028-1037.
31 Ding BS, Nolan DJ, Butler JM, *et al.* Inductive angiocrine signals from sinusoidal endothelium are required for liver regeneration. *Nature* 2010; **468**:310-315.
32 Muzumdar MD, Tasic B, Miyamichi K, Li L, Luo L. A global double-fluorescent Cre reporter mouse. *Genesis* 2007; **45**:593-605.
33 Ozerdem U, Grako KA, Dahlin-Huppe K, Monosov E, Stallcup WB. NG2 proteoglycan is expressed exclusively by mural cells during vascular morphogenesis. *Dev Dyn* 2001; **222**:218-227.
34 Hellstrom M, Kalen M, Lindahl P, Abramsson A, Betsholtz C. Role of PDGF-B and PDGFR-beta in recruitment of vascular smooth muscle cells and pericytes during embryonic blood vessel formation in the mouse. *Development* 1999; **126**:3047-3055.
35 Nehls V, Denzer K, Drenckhahn D. Pericyte involvement in capillary sprouting during angiogenesis *in situ*. *Cell Tissue Res* 1992; **270**:469-474.
36 Nehls V, Drenckhahn D. The versatility of microvascular pericytes: from mesenchyme to smooth muscle? *Histochemistry* 1993; **99**:1-12.
37 Snippert HJ, van der Flier LG, Sato T, *et al.* Intestinal crypt homeostasis results from neutral competition between symmetrically dividing Lgr5 stem cells. *Cell* 2010; **143**:134-144.
38 Mahmoud M, Allinson KR, Zhai Z, *et al.* Pathogenesis of arteriovenous malformations in the absence of endoglin. *Circ Res* 2010; **106**:1425-1433.
39 Stahl A, Connor KM, Sapieha P, *et al.* The mouse retina as an angiogenesis model. *Invest Ophthalmol Vis Sci* 2010; **51**:2813-2826.
40 Welch-Reardon KM, Wu N, Hughes CC. A role for partial endothelial-mesenchymal transitions in angiogenesis? *Arterioscler Thromb Vasc Biol* 2015; **35**:303-308.
41 Maddaluno L, Rudini N, Cuttano R, *et al.* EndMT contributes to the onset and progression of cerebral cavernous malformations. *Nature* 2013; **498**:492-496.
42 Peinado H, Olmeda D, Cano A. Snail, Zeb and bHLH factors in tumour progression: an alliance against the epithelial phenotype? *Nat Rev Cancer* 2007; **7**:415-428.
43 Piera-Velazquez S, Li Z, Jimenez SA. Role of endothelial-mesenchymal transition (EndoMT) in the pathogenesis of fibrotic disorders. *Am J Pathol* 2011; **179**:1074-1080.
44 Zeisberg EM, Tarnavski O, Zeisberg M, *et al.* Endothelial-to-mesenchymal transition contributes to cardiac fibrosis. *Nat Med* 2007; **13**:952-961.
45 Cooley BC, Nevado J, Mellad J, *et al.* TGF-beta signaling mediates endothelial-to-mesenchymal transition (EndMT) during vein graft remodeling. *Sci Transl Med* 2014; **6**:227ra234.
46 Medici D, Shore EM, Lounev VY, Kaplan FS, Kalluri R, Olsen BR. Conversion of vascular endothelial cells into multipotent stem-like cells. *Nat Med* 2010; **16**:1400-1406.
47 Cheng SL, Shao JS, Behrmann A, Krchma K, Towler DA. Dkk1 and MSX2-Wnt7b signaling reciprocally regulate the endothelial-mesenchymal transition in aortic endothelial cells. *Arterioscler Thromb Vasc Biol* 2013; **33**:1679-1689.
48 Humphreys BD, Lin SL, Kobayashi A, *et al.* Fate tracing reveals the pericyte and not epithelial origin of myofibroblasts in kidney fibrosis. *Am J Pathol* 2010; **176**:85-97.
49 Lin SL, Kisseleva T, Brenner DA, Duffield JS. Pericytes and perivascular fibroblasts are the primary source of collagen-producing cells in obstructive fibrosis of the kidney. *Am J Pathol* 2008; **173**:1617-1627.
50 Armulik A, Genove G, Betsholtz C. Pericytes: developmental, physiological, and pathological perspectives, problems, and promises. *Dev Cell* 2011; **21**:193-215.
51 Birbrair A, Zhang T, Wang ZM, Messi ML, Mintz A, Delbono O. Pericytes at the intersection between tissue regeneration and pathology. *Clin Sci* 2015; **128**:81-93.
52 Sims DE. Diversity within pericytes. *Clin Exp Pharmacol Physiol* 2000; **27**:842-846.
53 Etchevers HC, Vincent C, Le Douarin NM, Couly GF. The cephalic neural crest provides pericytes and smooth muscle cells to all blood vessels of the face and forebrain. *Development* 2001; **128**:1059-1068.
54 Simon C, Lickert H, Gotz M, Dimou L. Sox10-iCreERT2: a mouse line to inducibly trace the neural crest and oligodendrocyte lineage. *Genesis* 2012; **50**:506-515.
55 Raza A, Franklin MJ, Dudek AZ. Pericytes and vessel maturation during tumor angiogenesis and metastasis. *Am J Hematol* 2010; **85**:593-598.
56 Sarkes D, Rameh LE. A novel HPLC-based approach makes possible the spatial characterization of cellular PtdIns5P and other phosphoinositides. *Biochem J* 2010; **428**:375-384.
57 Rios AC, Fu NY, Lindeman GJ, Visvader JE. *In situ* identification of bipotent stem cells in the mammary gland. *Nature* 2014; **506**:322-327.
58 Claybon A, Bishop AJ. Dissection of a mouse eye for a whole mount of the retinal pigment epithelium. *J Vis Exp* 2011 Feb 27. doi:10.3791/2563

(**Supplementary information** is linked to the online version of the paper on the *Cell Research* website.)